A chemically defined and xeno-free hydrogel system for regenerative medicine.

John Ong [1,2,3], George Gibbons [4], Lim Yee Siang [5], Zhou Lei [3], Junzhe Zhao [1], Alexander W. Justin [1], Federico Cammarata [1], Ravisankar Rajarethinam [6], Colleen Limegrover [4], Sanjay Sinha [7*], Andras Lakatos [4*], Foad J. Rouhani [8*], Dan Yock Young [3*], Athina E. Markaki [1*]

* *denotes senior authorship.*

[1] Department of Engineering, University of Cambridge, UK

[2] School of Clinical Medicine, University of Cambridge, UK

[3] Department of Medicine, National University of Singapore, Singapore

[4] John van Geest Centre for Brain Repair, University of Cambridge, UK

[5] Genomic Institute of Singapore, Singapore

[6] Institute of Molecular and Cell Biology, Singapore

[7] Cambridge Stem Cell Institute, University of Cambridge, UK

[8] Wellcome Sanger Institute, Wellcome Genome Campus, Cambridge, UK

Correspondence:
Professor Athina E. Markaki
Department of Engineering
University of Cambridge
Trumpington Street
Cambridge CB2 1PZ
United Kingdom
Tel: +44-1223 332600,
Email: am253@cam.ac.uk

Dr John Ong
Clinical Lecturer in Hepatology
School of Clinical Medicine
University of Cambridge
Addenbrooke's Hospital, Hills Road
Cambridge CB2 0SP
United Kingdom
Tel: +44-1223 336700
Email: jo401@cam.ac.uk

ABSTRACT (140 words)

Bio-fabricated scaffolds facilitate bona fide cellular interactions, cell-type specification, and the formation of three-dimensional tissue architecture from human pluripotent stem cells (hPSCs). However, poorly defined xenogenic and non-clinically approved synthetic biomaterials greatly hinder translation into clinical therapy. Here we describe a protein screen-based hydrogel system made from widely available clinical-grade components. We show that Alphagel, a base hydrogel synthesized from human embryonic matrices, supported trilineage hPSC differentiation and was biocompatible *in vivo*. Further, by adding select proteins found in the maturing foetal liver, the resulting hydrogel (Hepatogel) enhanced the differentiation of hPSC-derived hepatocytes (H-iHeps) compared to Matrigel, a generic hydrogel. Importantly, when H-iHeps and Hepatogel were injected into the liver of immunocompromised mice, cell engraftment rates were significantly improved. Altogether, our customisable and clinically translatable hydrogel system provides a useful tool for developing organ-specific and effective therapies for regenerative medicine.

INTRODUCTION

Three-dimensional (3D) stem cell and organoid platforms recapitulate *in vivo* cellular and biomechanical interactions better than two-dimensional culture systems, enabling the development of novel diagnostics and therapeutics for disease (1,2). The spatial arrangement of stem cells and niche factors orchestrated by bio-fabricated scaffolds promote the self-organisation of cell masses and the formation of early organoids for tissue development. This geometry controls organoid patterning (3) and remains an important factor that underpins our capability to engineer whole organs in vitro. Human pluripotent stem cells (hPSC), which comprise induced pluripotent stem cells (iPSCs) and embryonic stem cells (ESCs), have the potential to generate any cell type in the human body. However, clinically suitable biomaterials for 3D hPSCs culture and differentiation are lacking and this paucity significantly limits regenerative medicine and tissue engineering.

Presently, Matrigel and Matrigel-derived matrices are often used to culture hPSCs and organoids derived from bi- or multi-potent adult stem cells. This is problematic because of widely recognised problems with the mouse sarcoma-derived matrix. Poor definability (4,5), batch-to-batch variability in growth factor concentrations (6,7), composition (8) and physical properties (7), immunogenicity (9), and pathogen transmission (10) are widely recognised. Synthetic biomaterials such as polyethene glycol (PEG), polyacrylic acid (PAA), polycaprolactone, or polyacrylamide (PAAm) have been explored (11), however, challenges in synthesising the desired derivatives limit clinical applications (4,12,13). Importantly, synthetic biomaterials frequently lack the biological niche factors which while avoiding unwanted matrix interactions, also lack the necessary biochemical cues for efficient hPSCs culture and differentiation (11,14). Furthermore, methods used to polymerise synthetic hydrogels frequently restrict cell transplantation where therapeutic injections, gelation and retention at target sites are preferred for ease of delivery (4,15). Recently, attempts have been made to conjugate deconstructed components of Matrigel with inert polymeric backbones (16,17). However, these are not suitable for hPSC culture and adversely affect stem cell pluripotency (18–20).

To address these issues, we developed a xenofree and clinically compatible system that mimics the different stages of embryonic development and organogenesis. We

hypothesised that hPSC-derived target cells would recapitulate primary cells better in customised hydrogels comprising organ-specific matrices rather than generic biomaterials like Matrigel or synthetic hydrogels. In that vein, we aimed to develop a liver extracellular matrix (ECM)-specific hydrogel as a proof-of-concept. Through a reductionist approach, we performed a protein screen and created a base hydrogel (termed “Alphagel”) that supported hPSC culture and trilineage differentiation in 3D. We then added select proteins found in maturing liver ECM to Alphagel. The resulting hydrogel, termed “Hepatogel”, produced hPSC-derived hepatocytes that were closer to maturing human hepatocytes than Matrigel, and it improved the engraftment of hPSC-derived hepatocytes when injected into the livers of immunocompromised mice. A summary of the workflow is illustrated in Fig.1(A). Herein, we contribute evidence that organ-specific hydrogels produce better end-target cells compared to generic hydrogels, and this system is a useful tool for developing organ-specific and effective therapies for regenerative medicine.

RESULTS

Protein screen reveals Laminin 521 and Fibrinogen as key candidates

To identify common and critical components in the embryological and foetal liver niche for components of a hydrogel, we first conducted a high throughput screen of a protein library (21). We first optimised an automated high throughput imaging pipeline to identify single cells by nuclear area, Fig.1(B), and then by mean fluorescent intensities (MFI) of nuclear markers of stem cell pluripotency (NANOG, SOX2, and OCT4) to characterise healthy hPSCs, Fig.1(C). At certain primary and secondary antibody concentrations, we found specific MFIs cut-offs were discriminatory against negative controls (human fibroblasts). For example in secondary antibodies for NANOG, 1:500 was differentially diagnostic but 1:1000 was not. In addition, nuclear measurements improved readouts by enabling machine learning and analysis, excluding “bright” cell clusters that often falsely elevated MFIs. The final pipeline produced a Stemness Index (SI) ranging from 0 (poorest performance) to 1 (best performance for maintaining pluripotency). This demonstrated excellent discriminatory ability (AUC 0.977, CI: 0.976-0.977, $p<0.0001$) being able to discern hPSCs from fibroblasts, Fig.1(D), and normal hPSCs from spontaneously differentiated islands of hPSCs after prolonged culture, Fig.1(E). Using this construct, we exposed hPSCs to the various niche

proteins and other scaffold-forming polymeric proteins to identify candidates. Liver niche proteins included in our screen were identified using proteomics-derived data from the human Matrisome Project (http://matrisomeproject.mit.edu) and our analysis of human fetal, paediatric, and adult livers (21).

We found select proteins present in both the embryological and fetal niche and some of these could replace Matrigel as a substrate for stem cell culture. An example of a short-term (1 week) screening panel is illustrated in Fig.1(F). However, the best candidate was chosen for its ability to maintain the highest SI in hPSCs after prolonged culture; Laminin 521 had the highest SI (between 0.95 to 1.0) after 3-4 months in culture. Thus, we sought to combine Laminin 521 with a polymeric backbone to obtain a 3D scaffold since a pure or physiologically relevant Laminin 521 hydrogel is not currently available. We found human fibrinogen was the best polymeric protein for pairing with Laminin 521 because of its mechanical tunability and it did not cause the rapid and spontaneous differentiation of hPSCs. Notably, the other polymeric backbones such as albumin and collagen that we investigated either resulted in poor hPSC attachment (22) or it triggered spontaneous differentiation of hPSCs (Supplementary Figure 1).

Optimising fibrin-laminin hydrogels to support hPSC growth in vitro

To determine the optimum conditions for culturing hPSCs in 3D, we evaluated different compositions of Laminin 521-enriched fibrin hydrogels (FLGs) versus fibrin hydrogels (FGs) as controls. We found both categories of hydrogels displayed distinctive characteristics. In 2D cell culture, cell attachment and expansion were noticeably better in FLGs (70-100% confluence) versus FGs (10%-20% confluence) after 4-5 days in culture, Fig.2(A). In 3D cell culture, higher fibrinogen with lower laminin concentrations resulted in poor colony expansion and “dark” unhealthy hPSC colonies compared to Matrigel; widely recognised features of spontaneous differentiation in hPSC culture (23–25). This was corroborated across several conditions by a significant decrease in SOX2, NANOG, OCT4 MFIs, and SI compared to hPSCs grown on Matrigel in 2D culture as standard practice (Supplementary Figure 2). Nonetheless, the optimal balance between fibrinogen, thrombin and laminin concentrations was identified by a combination of SI in hPSCs and the stability of FLGs in cell culture; hydrogels with low fibrin concentrations ($\leq$ 1mg/ml) disintegrated after

a week in cell culture. This optimum ratio (50%:50% v/v Laminin 521 and 2.5mg/ml fibrin hydrogel) was termed “Alphagel”. Alphagel was found to be up to a third more cost-effective than Matrigel for 3D hPSC cell culture (Supplementary Figure 3). Unlike other compositions of FLGs, Alphagel supported the healthy expansion of hPSCs into 3D cell aggregates closely resembling embryoid bodies (EBs), Fig.2(B).

To visualise the differences between fibrin-only hydrogels and Alphagel, scanning electron microscopy (SEM) was performed on acellular hydrogels. This demonstrated smaller pores and thinner fibrin fibres as previously observed in laminin-fibrin hydrogels (26,27). However, thin membranes in between inter-connecting fibrin fibres in Alphagel were observed and these were absent in fibrin-only hydrogels; Fig.2(C) and Fig.2(D). As protein concentration alters the elastic properties of hydrogels, we next measured Young’s modulus of fibrin-only hydrogels, FLGs, and Alphagel. We found that hydrogel stiffness increased significantly with laminin and fibrin concentrations; Fig.2(E). The Young’s modulus in FLGs containing 1.5mg/ml fibrin was higher compared to 1.5mg/ml fibrin-only hydrogels (fold increase 3.6 ± 0.6, $p < 0.0001$) and 2.5mg/ml fibrin-only hydrogels (fold increase 2.6 ± 0.2, $p < 0.0001$). Despite the increase in stiffness, cell viability was notably higher in Alphagel compared to fibrin-only hydrogels (98.7 ± 0.3% vs 80.8% ± 8.3% respectively, $p <0.05$); Fig.2(F). There were no significant differences in cell viability across Alphagel and the 2D substrates.

Next, to determine if the FLG hydrogels were stable, we measured the amount of Laminin 521 that was leached from acellular Alphagel into the culture media over time. This showed that the greatest loss of Laminin 521 from the hydrogel occurred during the first 24 hours of conjugation (approximately 3% leached into media). Thereafter, the leaching of Laminin 521 into the culture media was negligible and approximately 97% of the laminin remained within the hydrogel after 9 days; Fig.2(G) and Fig.2(F).

Alphagel supported 3D hPSC culture and enabled directed 3D differentiation.

To optimise the culture conditions of hPSC in 3D, we first tested the performance of hPSC-laden Alphagel paired with different stem cell maintenance media over 2 months. Stem cell culture media E8™, TeSR-E8 ™, mTeSR™ 1, mTeSR™ Plus, and TeSR™ 2 were used. We found the best stem cell culture media that maintained

markers of hPSC pluripotency with Alphagel were the TeSR-only family i.e. TeSR™ 2, mTeSR™ 1 and mTeSR™ Plus, yielding SIs of hPSCs between 0.95 to 1.0; Supplementary Figure 2(A). Despite prolonged culture, markers of pluripotency (OCT4, NANOG, and SOX2) were still strongly expressed in the 3D hPSCs aggregates. For validation, these aggregates were dissociated into smaller cell clusters and grown as a single cell layer in 2D. Importantly, these hPSCs continued to proliferate in 2D and expressed all 3 pluripotent nuclear markers (Supplementary Figure 4). Next, to fully demonstrate pluripotency, we cultured hPSCs in Alphagel (3D) and then performed 3D differentiation of hPSCs into all three germ cell lines; mesoderm (heart), ectoderm (neurons), and endoderm (liver).

During cardiac specification, hPSC aggregates in Alphagel successfully proliferated and formed 3D contractile cardiac tissue after the initiation of cardiac differentiation; Fig 3(A) and Supplementary Movie 1. Immunofluorescent staining (IF) of cells for the cardiac marker Troponin T (TnT) and the general myoblast marker α-SMA (28) was strongly positive; Fig 3(B). Cardiomyocytes were observed to start beating at a rate of 30 to 50 beats/min between Day 5 to Day 8 of the cardiac differentiation process; early contractions were weak and asynchronous (Supplementary Movie 1). However, the contractility rate increased to 60 ─ 80 beats/min minute, and contractions were noticeably stronger and synchronous by Day 12 ─ 14 (Supplementary Movie 2). There was no significant difference in differentiation efficiency (proportion of TnT positive cells) between Alphagel and Matrigel (75.4 ± 18.5% vs 78.2 ± 15.4% respectively, $p = 0.14$). In fibrin-only hydrogels, the differentiation efficiency was significantly lower versus Alphagel (34.9 ± 21.3%; $p < 0.001$); Supplementary Figure 5(A).

For neuronal specification, hPSCs were subjected to a commonly applied protocol utilizing dual-SMAD inhibition (29,30). For comparison, both a fibrin-only control and an aggregate-based (neurosphere) method were included. At Day 16, all conditions showed successful acquisition of a neural fate as demonstrated by co-expression of the neuroepithelial progenitor markers SOX2, nestin, and β-catenin; Fig.3(C) and Supplementary Figure 5. Quantifications at this time point showed comparable cell composition of SOX2 immunoreactive (IR) progenitor cells in Alphagel (79.5 ± 5.0%) and neurospheres (82.4 ± 9.3%) conditions. In the fibrin-only condition, there were slightly fewer SOX2 IR cells (74.1 ± 12.6%) however this difference was not statistically

significant; Supplementary Figure 5(B). To ascertain if the structural properties of Alphagel could improve the organization and morphology of differentiated neuroepithelia, we determined the number and size of lumens demarcated by nestin/β-catenin co-labelled apical cells and compared to that seen in fibrin-based hydrogels and neurospheres. We found that the frequency of polarized areas (approximately 0.03/mm^2) was consistent across all conditions, albeit less variable under hydrogel conditions; Supplementary Figure 5(C). However, the average lumen area was significantly increased in hydrogel conditions with Alphagel (403.29 µm^2; $p = 0.0007$) versus neurospheres (105.46 µm^2); Fig.3(D).

For hepatic specification, successful differentiation of hPSCs into hepatocytes (iHeps) was demonstrated through IF staining, showing previously established gene expression signatures (31), and functional assays. Positive IF staining for hepatocyte markers Albumin, HNF1A, HNF4A, CYP2A6, CD147, and E-cadherin was demonstrated in 3D differentiated cells, Fig.3(E). Similarly, key hepatocyte markers HNF4A, CEBPA and CYP3A4 were shown to be expressed in iHeps derived in Alphagel at the levels as iHeps derived in Matrigel; Fig.3(F). However, CYP3A7 and AFP expression were significantly higher in Alphagel and Matrigel compared to adult primary human hepatocytes (PHH); $p < 0.0001$ for both, Fig.3(F). Notably, TBX3 expression was also high in Alphagel and Matrigel but there was no statistically significant difference when compared to PHH. For further characterisation, 18 other hepatocyte-related genes were analysed (Supplementary Figure 6). 10 of 18 genes showed differences between PHH and Alphagel-derived hepatocytes. Specifically in the latter, BAAT, ABCC2, and TAT were down-regulated whilst CYP3A5, GATA4, GATA6, FOXA1, SOX9, LGR5, and CK19 were up-regulated compared to PHH (p values in Supplementary Figure 6).

To assess the functionality of iHeps derived in Alphagel, albumin secretion, cytochrome 3A4 activity, LDL update, as well as CDFDA uptake and excretion were investigated at the end of the hepatic differentiation process. Albumin, a key marker of hepatocyte synthetic function, was found to be secreted in similar amounts by PHH and iHeps cultured in Alphagel and Matrigel; Fig 3(G). However, CYP3A4 activity was lower in Alphagel and Matrigel than PHH as reported by other groups (31,32); Fig 3(G). Importantly, low-density lipoprotein (LDL) uptake and 5-(and-6)-Carboxy-2',7'-

Dichlorofluorescein Diacetate (CDFDA) secretion, both features of hepatocyte metabolic function, were demonstrated in Alphagel; Fig.3(H) and Fig.3(I). These were also present in primary hepatocytes and hepatocytes derived in Matrigel. There was no statistically significant difference in differentiation efficiency between Alphagel and Matrigel (defined herein by the proportion of albumin-positive cells). This was approximately 70.6% and 69.9% respectively ($p=0.73$). In fibrin-only hydrogels, the differentiation efficiency was significantly lower versus Alphagel (28.8%, $p<0.0001$); Supplementary Figure 7(A).

Fibrin-laminin hydrogels demonstrated good biocompatibility *in vivo*

Having demonstrated tri-lineage differentiation of hPSCs in Alphagel, we next sought to determine if Alphagel and fibrin-laminin hydrogels were biocompatible as a potentially injectable biomaterial for clinical use. To that end, we injected immune-competent Black 6 (C57BL/6) mice subcutaneously with Alphagel (test group), 0.9% saline (negative control), and 1.0% v/v croton oil (inflammatory agent, positive control) to assess for an immune response; n=3 for each group and time point. Mice were observed and culled over 6 weeks. Histology results showed that mice injected with Alphagel had mild inflammation at the site of injection between 1 to 2 weeks; Fig 4(A). However, this resolved completely between 4 to 6 weeks; Supplementary Figure 7(B). Mice injected with 0.9% saline also had inflammation at the injection site after 1 week although this was minimal and resolved completely by 2 weeks. Mice injected with 1% croton oil developed ongoing severe inflammation which progressed to wound dehiscence by 6 weeks; these mice were culled humanely when wound inflammation became visibly severe. Histological slides were scored objectively by a histopathologist blinded to the groups using an international scoring tool (Supplementary Figure 8) and graded using standardised nomenclature (33–35). Neoplasia was not observed at the injection sites. The improving histological scores were consistent with the qualitative reporting of the histological slides, Fig.4(B), providing evidence that fibrin-laminin hydrogels were biocompatible and biodegradable *in vivo*.

FLGs enriched with liver-specific ECM enhanced the phenotype of iHeps

Next, to test our hypothesis that hydrogels enriched with organ-relevant ECM can improve stem cell-derived phenotypes, we added Laminin 411 and Laminin 111 to

Alphagel. These were specific ECMs we found to be important in liver development (21). Various combinations of protein concentrations were tested and the optimum concentration of Laminins 521, 411 and 111 was termed “Hepatogel”. iHeps derived in Hepatogel, Alphagel and Matrigel were compared against PHH using the above panel of liver-specific genes and functional assays. Key changes in the gene expression profile are highlighted in Fig.4(C). Briefly, Hepatogel increased the gene expression of Transferrin (TF) versus Alphagel (1.5 ± 0.4 fold increase, $p < 0.0001$) and PHH (2.2 ± 0.6 fold increase, $p < 0.001$). Gamma GT (GGT) gene expression was significantly increased across all three hydrogels compared to PHH but it was highest in Hepatogel (3.3 ± 0.3 fold increase vs PHH, $p < 0.05$). G6PC gene expression in Matrigel was significantly lower versus PHH (-6.7 ± 0.6 fold lower, $p < 0.05$), however, expression in Hepatogel was comparable to PHH. Bipotent-hepatoblast marker LGR5 was significantly upregulated in Alphagel (6.0 ± 0.6 fold increase; $p<0.01$) and Hepatogel (6.5 ± 0.5 fold increase; $p < 0.01$) versus PHH. Importantly, expression of immature fetal liver markers CYP3A7 and AFP were significantly lower in Hepatogel versus Matrigel (1.8 ± 0.4 fold decrease; $p < 0.05$ and 1.3 ± 0.1 fold decrease; $p < 0.05$, respectively). The remaining results of the hepatocyte gene panel are attached in Supplementary Figure 9.

The synthetic function of hepatocytes was assessed by albumin secretion. Hepatogel was found to induce the highest albumin secretion compared to Alphagel, PHH, and Matrigel; Fig.4(D). The metabolic function of hepatocytes was assessed by CYP3A4 activity and Apolipoprotein B (APOB) secretion. CYP3A4 activity was highest in PHH. iHeps derived in Hepatogel had higher CYP3A4 activity than Alphagel (2.4 ± 0.1 fold increase; $p < 0.05$) and Matrigel. However in the latter, the increase was marginal and not statistically significant (1.2 ± 0.5; $p = 0.47$), Fig.4(E). APOB secretion was higher in Hepatogel compared to PHH however there were no differences between Hepatogel and Alphagel. In summary, the two liver-relevant ECM added to Alphagel resulted in higher TF expression, CYP3A4 activity, and Albumin secretion compared to Alphagel alone. Interestingly, up-titrating Laminin 411 concentrations in Hepatogel significantly increase APOB secretion. Conversely, this promoted the formation of branching 3D tubular structures with a corresponding rise in Alkaline Phosphatase (ALP) in the culture media (Supplementary Figure 10). Interestingly, these structures were lined

with cells which expressed biliary markers CK7, CK19, and SOX9 (Supplementary Figure 11, Supplementary Movie 3 and Supplementary Movie 4).

Hepatogel improves the engraftment of transplanted hepatocytes

Since iHeps cultured in Hepatogel (H-iHeps) had a better synthetic and metabolic profile than Alphagel, we next investigated if by introducing a proliferative/regenerative liver niche at the site of transplantation, the engraftment of transplanted hepatocytes could be improved. Currently, hepatocyte engraftment rates in cell therapy are poor, and Matrigel and its derivatives, are not permitted in clinical use. To that end, we injected H-iHeps in Hepatogel and H-iHeps in solution (standard practice) directly into normal livers of immune-compromised mice (NSG^{TM} mice, n=6 each group per time point, 3 time points). Mice were monitored for human albumin in their serum and then culled for liver histology. Three days after intrahepatic injections, the first group of mice were culled and examined. It was obvious on post-mortem that H-iHeps transplanted in Hepatogel were still present at the injection site, and this was much more evident compared to H-iHeps delivered in solution (0.9% Saline); Fig.5(A). Respectively, this corresponded to significantly higher H-iHeps cell numbers in mice liver histology and higher human albumin concentrations in mice serum; Fig.5(B) to Fig.5(D). Notably, human albumin remained detectable in mice transplanted with H-iHeps and Hepatogel at Day 6 whereas in mice transplanted with H-iHeps in solution, it was undetectable after the second day. Nonetheless, beyond 8 days human albumin decreased significantly and was undetectable in both groups. When the remaining mice in both groups were culled at 7 days and 2 months after transplantation, no H-iHeps colonies or tumours were seen at the injection sites, demonstrating the clearance of injected H-iHeps.

DISCUSSION

In this work, we found that a select group of physiologically relevant proteins could be used as biomaterials for 3D hPSC culture. Importantly, we observed that organ-specific hydrogels can produce better end-target phenotypes compared to Matrigel and its derivatives; a generic mouse sarcoma-derived substrate. This was evidenced by significantly higher albumin expression paired with lower fetal liver markers CYP3A7 and AFP in hepatocytes derived from Hepatogel compared to Matrigel. ECM

properties vary from organ to organ, in health and disease. Although 2D stem cell culture and organoid technology were established using Matrigel as a central substrate, compositional and mechanical differences to physiological ECM likely contribute to immature phenotypes compared to adult primary cells (36). Importantly, Matrigel derivatives are not approved for clinical use and thus Alphagel is an alternative for 3D hPSC culture and differentiation where hPSCs can be used to derive all cell types in an organ for tissue engineering. In that vein, alternative substrates for hPSC culture, Laminin 521 and vitronectin, are not readily available as pure 3D hydrogels. Laminin 521 has recently been conjugated with silk (Biosilk, Biolamina) to form a generic hydrogel for 3D stem cell and organoid culture. However, silk is not native to the human ECM and Biosilk is not licensed for clinical use. Notably, some hPSC differentiation protocols using vitronectin require the dissociation of cells mid-process as well as a change in the substrate (37); this disrupts any early 3D structures that may form in vitro.

We found that the combination of high Laminin 521 concentrations with low fibrinogen concentrations was a good pairing to create a novel hydrogel for 3D hPSC culture. Physiologically, Laminin 521 and 511 are present in the inner cell mass of the blastocyst and its basement membranes during embryological development (38,39). Its expression remains constant throughout inner cell mass expansion and during differentiation whereas Laminin 511 expression decreases during differentiation (39). Importantly, through RNAreq of human adult and foetal liver tissue (21), we had established that Laminin 521 is differentially expressed in the maturing fetal liver, along with a small group of ECM proteins that also support stem cell pluripotency to some extent; Fig.1(F). Notably, Fibrinogen is produced by trophoblasts during early development (40,41), and has the potential for use as an injectable biomaterial being abundantly present in human serum. Cell and protein adhesion is supported by arginine-glycine-aspartate (RGD) binding motifs at positions 96 and 572-574 on the α chains, heparin-binding domains (HBDs) also on the α chains, and a carboxy-terminal peptide (HHLGGAKQAGDV) at position 400-11 on the γ chains (42,43). Likewise, multiple binding sites on the α chains (RGD and HBD) and β chains (mainly RGD) in laminins facilitate cell and protein adhesion (44,45).

Nonetheless, there are conflicting data on the effects of fibrin hydrogels on stem cell culture. Gandhi et al (46) reported that fibrin gels (30mg/ml) could be used for iPSC culture. Notably, fibrin concentration is directly proportional to the stiffness of fibrin matrices. Our FLGs were finetuned to a stiffness of ~ 250-400 Pa to mimic the stiffness of embryological liver (47,48) and the 10 mg/ml fibrin-only gels that we tested had a stiffness of ~ 1.7-.1.9 kPa. In our experience, high concentrations of fibrin (≥ 4 mg/ml) promoted spontaneous differentiation across 3 hPSC cell lines (2 ESC cell lines and 1 iPSC cell line) and this was augmented by the type of stem cell maintenance media used (Supplementary Figure 2). This was evidenced by the low differentiation efficiency and sub-optimal end-target cell phenotypes in fibrin-only hydrogels (e.g. our hepatic differentiation results Fig.3 and Fig.4). and independent studies that showed compliant substrates maintain self-renewal of ESCs by downregulating cell-matrix tractions whilst stiffer substrates promote spontaneous differentiation with downregulation of OCT3/4 expression (49,50). Interestingly, Liu et al (50) demonstrated that compliant fibrin-only gels (1mg/ml, ~ 100 Pa) promoted the selection and growth of tumour cells that express stem cell markers CD133, Nestin, BMI-1, C-kit but not stem cell markers OCT3 and NANOG. In our study, the addition of Laminin 521 to low-concentration fibrin matrices preserved high OCT4 and NANOG expression in hPSCs over prolonged culture (2-3 months), and similarly fibrin-only hydrogels resulted in absent OCT3 and NANOG expression. Furthermore, no tumour growth was observed after H-iHeps were transplanted into the NSG^{TM} mice. In that vein, the mild local inflammation in the immunocompetent Black 6 mice was likely a combination of iatrogenic injury (given similar reactions with saline injections) and the implantation of xenogeneic biomaterials (human ECM proteins). Nonetheless, the mild degree of inflammation and its complete resolution by 6 weeks indicates good biocompatibility that would likely be tolerated well in human studies.

Since the benefits of fibrin-only matrices are limited in hPSC culture, several groups have recently attempted to create ECM-enriched fibrin hydrogels for regenerative medicine and cell therapy. Laminin 111 enriched fibrin matrices, loaded with (27,51) and without (52,53) cells were used to promote musculoskeletal regeneration after injury. Interestingly, Broguiere et al (16) attempted to mimic Matrigel by enriching fibrin gels with laminin 111 and collagen IV; they then demonstrated it could support the growth of adult stem cells (ASCs) through the propagation of cystic gastrointestinal

organoids (intestinal, pancreatic and hepatic organoids). In our experiments, we found that Laminin 111 could maintain hPSC pluripotency, Fig.1(F); however, over limited passages. hPSCs cultured on Laminin 111 were observed to change morphology and form colonies of spontaneously differentiated cells within 1-2 weeks (Supplementary Figure 12). Independently, several groups have also concluded that Laminin 111 triggers the spontaneous differentiation of hPSCs; likely through the α1 chain and β1 chain binding to the α3β1-integrin receptor (18–20). Therefore, hydrogels highly enriched with Laminin 111 may be used for ASCs but these are likely to cause phenotypic instability with hPSCs. In our experiments, differentiation efficiency varied between hPSC cell lines, however, these were similar in the reported literature (54–56).

The organization and polarization of tissues are important to tissue function. In particular, this has been a defining feature previously optimized in neural organoid protocols (57). While these methods are typically reliant on embedding early aggregates in Matrigel, we show that Alphagel has similar properties, allowing the spontaneous development of organized neural tissue with enlarged apical lumens. Besides consistency, a major advantage of the Alphagel system is that it allows simultaneous differentiation and structural organization without the need for further physical manipulations or tedious time-consuming steps, and thus could be useful to explore as a substrate for brain organoid generation. Similarly, we show the platform is useful in generating 3D cardiac tissue without the need for substrate changes mid-differentiation, thus holding promise in the development of injectable regenerative therapies for cardiac disease or ex vivo cardiac tissue engineering.

Finally, we demonstrated that Hepatogel improves the engraftment efficiency of H-iHeps in murine livers, highlighting its potential for use as cell therapy for liver disease. At present, human hepatocytes are commonly delivered in solution via injections either directly into the liver or at various vascular sites that feed directly into the liver for cell therapy (58). However, in these approaches, engraftment rates are poor (58,59). Transplanted hepatocytes commonly occupy microvascular spaces, and the resulting ischaemic injury triggers vascular and immune responses within the local niche which usually has a deleterious effect on the transplanted cells (59). This limits cell engraftment, treatment efficacy and the broader use of cell therapy in liver disease.

Other methods of cell delivery involve the injection of cells encapsulated with degradation-resistant matrices such as alginate into the abdomen (60). This is often a temporising measure to bridge patients with liver failure to liver transplantation, in this situation the encapsulation limits cell engraftment and repopulation. Therefore, we evaluated if biomaterials (Hepatogel) could improve the engraftment rates of transplanted iHeps by replacing the hostile environment with a “regenerative” liver niche. To that end, we show that H-iHeps transplanted into mice liver engrafted better with Hepatogel than H-iHeps in solution. This was evidenced by the post-mortem findings, higher H-iHep cell counts, and the level of human albumin in mice serum after transplantation; Fig.5(A) to (D). However, even though Hepatogel improved engraftment, H-iHeps did not proliferate to replace native hepatocytes in the host liver beyond one to two weeks. This may have been caused by the immunogenicity of hPSC cells (61), limitations of current iHep technology (62), or immunological responses in the recipient mice; NSG^{TM} mice have preserved neutrophils and monocyte function. Limited repopulation of transplanted iHeps remains a universal challenge and our long-term observations are similar to others reported in the literature (59). Nonetheless, as biotechnology advances, the derivation of high-quality non-immunogenic lab-derived hepatocytes will improve, and clinically applicable hydrogels will serve as useful adjuncts in hepatocyte derivation and cell therapy by improving cell delivery, engraftment, and treatment efficacy (15).

CONCLUSION

We have shown proof-of-concept that bioengineered organ-specific hydrogels can improve the phenotypes of hPSC-derived end-target cells compared to generic hydrogels. Our fully defined and liver-specific hydrogel (Hepatogel) increased gene expression and metabolic function in induced hepatocytes compared to Matrigel. Being biodegradable, injectable and comprising of clinical grade biomaterials, Hepatogel may serve as a useful clinical adjunct to improve hepatocyte engraftment for cell therapy.

MATERIALS AND METHODS

Protein Screening

Protein screening was performed using the Opera Phenix High-Content High-Throughput (HCHT) screening system (PerkinElmer, USA). Briefly, the MFI of OCT4,

NANOG, and SOX2, were measured in hPSCs (positive control) cultured on Geltrex (Thermofisher, #A1413302) and human fibroblasts (negative control) cultured on uncoated plates. Optimised antibody concentrations are listed below. Nuclear measurements were measured using DAPI. Differential characteristics between the two populations were used to identify thresholds for machine learning. A screening pipeline was created using Harmony High-Content Imaging and Analysis software (Perkin Elmer, USA) and validated for accuracy as reported. hPSCs were then plated on 96-well tissue culture-treated plates (Greiner Cellstar, #M0812) coated with single substrates at 4 different concentrations. The measure of pluripotency within a stem cell population was then defined as the "Stemness Index" (SI), which was calculated by:

$$\textit{Stemness Index (SI)} = \frac{\textit{Total number of Stem Cells Identified}}{\textit{Total number of Cells In Population}}$$

The maximum values of SI are 0 and 1, and the equation was incorporated into the pipeline. This enabled the automated calculation of results and identification of proteins that maintained stem cell pluripotency. Positive hits were checked using brightfield microscopy.

2D cell culture

hPSCs were maintained on Geltrex-coated plates in feeder-free mTeSR-1™ and mTeSR Plus™ media (Stemcell Technologies #85850 and #100-0276) using an established protocol (63). Geltrex was substituted for other substrates during protein screening. During maintenance, cells were split at 70-80% confluence using Accutase (Millipore, #SCR005), washed with DMEM/F12 (Life Technologies, #11330032) and re-seeded onto Geltrex-coated 6-well plates (Greiner, #657160) at a ratio of 1:6 to 1:8. 1mM Y27632 ROCK inhibitor (Stratech Scientific, #S1049-SEL-2mg) was used to increase cell attachment. Media was supplemented with penicillin and streptomycin (Millipore, #TMS-AB2-C). For screening experiments, human ESCs (KCL033) and human iPSCs (RMA and BOB cell lines) were used. These were gifted by Dr Tamir Rashid (King's College London). For other experiments, 2 ESC cell lines (H1 and H9, WiCell #WA01 and #WA09 respectively) and 1 episomal iPSC cell line (ThermoFisher,

#A18945) were used. Cell viability in 2D and 3D experiments was assessed using Trypan Blue (Sigma, #15250061).

Human dermal fibroblasts were available in-house (Sigma, #106-05a). Depending on experiments, these were cultured either on uncoated tissue culture flasks (Corning, #CLS3275) or Geltrex-coated 6-well plates. Fibroblasts were maintained in DMEM/F12 media (Life Technologies, #11330032), 10% foetal bovine serum (Sigma, #A9418), and 1% penicillin and streptomycin (Millipore, #TMS-AB2-C). Fibroblasts were passaged using Trypsin (ThermoFisher, #11538876).

Primary human hepatocytes from 3 different non-diseased donors were obtained commercially (Lonza, #HUCPI). These were quality-controlled, characterised and came from three different lots; Lot no. HUM182701, HUM182641, and HUM191381. Cells were thawed, plated on collagen-1 coated plates, and recovered for at least 24 hours in Hepatocyte Culture Media™ (HCM) including the complete HCM bullet kit (Lonza, #CC-3198) according to the supplier's protocol. Experiments commenced after 24 – 48 hours of cell recovery.

3D cell culture

hPSCs were cultured in 3D domes of Matrigel, fibrin-only gels, or FLGs plated on hydrophobic non-tissue culture-treated hydrophobic plates under normoxic conditions at 37°C. 50µl domes were used for 24-well plates (Sarstedt, #83.3922.500) or 25µl domes for 96-well plates (Ibidi, #89621). H1, H9 and episomal cell lines were used for these experiments. Feeder-free mTeSR-1™ and mTeSR Plus™ media (Stemcell Technologies #85850 and #100-0276) were used for routine stem cell maintenance. hPSCs designated for animal experiments were maintained in xeno-free TeSR™ 2 media (Stemcell Technologies, #05860). Cells were split every 5-6 days using TrypLE Express (Gibco, #12604013). Each dome required 20-25mins in TrypLE Express with manual pipetting for successful dissociation. Domes were then re-loaded with 12,500 to 225,00 cells depending on experiments.

For experiments investigating the effect of stem cell culture media on hPSC pluripotency in Alphagel, TeSR-E8™ culture media (Stemcell Technologies, #05990), E8™ culture medium (ThermoFisher, #A1517001), and TeSR-E8TM culture medium

(Stemcell Technologies, #05990) were used in addition to those described above. All culture media were supplemented with 1% penicillin and streptomycin (Millipore, #TMS-AB2-C). Media were refreshed on alternate days. EBs formed after three to four days in FLGs and Matrigel.

3D cardiac differentiation

hPSCs designated for cardiac differentiation were transitioned to E8™ culture medium (ThermoFisher, #A1517001) supplemented with 2.25 ng/ml of Fibroblast Growth Factor-2 (FGF-2: Qkine, #Qk053), and 1.74ng/ml of Transforming Growth Factor Beta (TGF-b: Bio-techne, #7754-BH). This media is primed for cardiac differentiation as previously described (64). When hESC colonies reached the desired number and size, cardiac differentiation was initiated using a previously established protocol (65). Briefly, mesodermal specification was initiated by replacing the FGF-2 and TGF-b enriched E8 maintenance media with CDM-BSA (Sanjay Sinha Lab, University of Cambridge) containing 20ng/ml of FGF-2/ml, 10μM of 2-(4-Morpholinyl)-8-phenyl-4 H-1-benzopyran-4-one (Ly294002: Promega, #V120A), 50ng/ml of Activin A (Stemcell Technologies, #78132.2), and 10ng/ml of Bone Morphogenic Protein-4 (BMP-4: RnD system, #314-BP-050). After 42 hours (Day 1.5), this was replaced with CDM-BSA containing 8ng/ml of FGF-2, 10ng/ml of BMP-4, 1μM of retinoic acid (Sigma, #R2625) and Wnt/β-catenin signalling inhibitor endo-IWR1 (R&D systems, #3532). Media was refreshed after 48 hours (Day 3.5). After another 48 hours (Day 5.5), the media was replaced with CDM-BSA containing 8ng/ml of FGF-2 and 10ng/ml of BMP-4. Standard CDM-BSA media was then refreshed every 48 hours (Day 7.5 onwards).

3D neuronal differentiation

hPSCs designated for neuronal differentiation were transitioned into Stem Flex media (ThermoFisher, # A3349401) with the addition of 10μM Y-27632 (Tocris, #1254) before initiating differentiation. Media was refreshed daily. When EBs were of sufficient number and size in Alphagel, neuronal differentiation was performed using an established protocol (66). Briefly, after four days of expansion in Alphagel with Stem Flex media, the media was switched to N2B27 media (in-house) supplemented with 5μM SB-431542 (Tocris, #1614), 200nM LDN-193189 (Miltenyi, #130-103-925), and 2μM XAV-939 (Tocris, #3748). Media with these factors was refreshed daily for ten days. After this, cells were maintained in N2B27 media only for a further six days.

3D hepatic differentiation

Hepatocyte differentiation was performed using a previously established protocol (63). Briefly, hPSCs were cultured in RMPI (ThermoFisher, #22400089) supplemented with 2% B27 minus insulin (ThermoFisher, #A1895601), 100ng/ml of Activin A, 20ng/ml of FGF-2 (ThermoFisher, #PHG0023) and 10ng/ml of Bone Morphogenic Protein-4 (BMP-4: R&D system, #314-BP-050) on differentiation days 1 — 2 to initiate differentiation. From differentiation days 3 — 5, the media was replaced with RMPI supplemented with 2% B27 minus insulin and 100ng/ml Activin A only. Hepatic endoderm specification was initiated on differentiation days 6 — 10 using RMPI supplemented with 2% B27 and insulin (ThermoFisher, #17504044), 10ng/ml FGF-2, and 20ng/ml BMP-4, followed by RMPI with 2% B27, insulin, and 20ng/ml hepatocyte growth factor (HGF: Peprotech, #100-39-250) on differentiation days 11 — 15. Maturation of hepatic endoderm was initiated on differentiation days 16 — 21 using complete HCM media supplemented with 10ng/ml Oncostatin M (OSM: R&D systems, # 8475-OM-050), 20ng/ml HGF and 0.1μM Dexamethasone (ThermoFisher, #A17590.06).

Synthesis of fibrin hydrogels

Human fibrinogen from non-diseased donors (Merck Millipore, #341576-1GM) was reconstituted in sterile 0.9% saline to a stock concentration of 67mg/ml. Human thrombin (Sigma, #T6884-100UN) was reconstituted in sterile 0.9% saline supplemented with human serum albumin (0.1% w/v) giving a stock concentration of 50U/ml. DMEM/F12 was then added to various volumes of fibrinogen and thrombin to achieve the desired final fibrinogen concentration of the fibrin gels. Final fibrinogen concentrations in the hydrogels that we tested ranged from 1mg/ml to 10mg/ml. The final concentration of thrombin in these hydrogels was maintained at 1U/ml. For cell experiments, hPSCs were loaded into the DMEM/F12 compartment.

Synthesis of Alphagel and Hepatogel

Alphagel and Hepatogel were synthesised using similar methods of fibrin-laminin enrichment previously reported (16,27) with minor adjustments. Briefly, for acellular Alphagel domes, human recombinant laminin 521 (Biolamina, #CT521-0501/LN521-05), human fibrinogen and DMEM/F12 were incubated in sterile Eppendorf (Elkay Lab,

#MICR-050) at 37ºC for 15 minutes. The mixture was then mixed and left to incubate for a further 15 minutes. Lastly, thrombin diluted in DMEM/F12 at room temperature was added to the mixture for gelation. 50µl domes of the final mixture were then plated on 24-well flat bottom hydrophobic plates (Sarstedt, #83.3922.500) using wide bore pipette tips (Starlab UK, #I1011-8000). The final composition of Alphagel contained a 50:50 v/v mixture of Laminin 521, 2.5mg/ml fibrinogen and 1U/ml thrombin. For Hepatogel, Laminin 411 (Biolamina, #LN411) and Laminin 111 (Biolamina, #LN111) were first purified using Amicon Ultra-0.5 centrifugal filter units (Merck Millipore, UFC5003) and reconstituted in sterile PBS. Then, Laminin 521, 411, and 111 were mixed in the respective ratio of 5:1:2. For cell experiments, hPSCs were loaded in the laminin(s)-DMEM/F12-fibrinogen compartment and incubated as described above. Lastly, the thrombin-DMEM/12 compartment was added for polymerisation. The cell-laden mixture was then seeded at 50µl per dome in 24-well plates and inverted to allow the cells to remain suspended in 3D. These plates were kept inverted for a further 30 minutes to allow to gelation complete fully. Thereafter, plates were turned over and 1ml of media was added to each well. Media was refreshed at a frequency determined by experiments.

Scanning Electron Microscopy (SEM)

Fibrin-only hydrogels and FLGs samples for SEM were prepared following a previously published protocol (67). Briefly, fibrin-only and FLGs were mounted and gelled in 444 ferritic stainless-steel scaffolds (Nikko Techno Ltd., Japan) for mechanical support. An hour after gelation, samples were fixed in 10% formalin (VWR International, #11699455) and left in a fume hood overnight. The following day, samples were washed three times with PBS and then dehydrated in increasing concentrations of ethanol-de-ionised (DI) water mixtures; 30, 50, 70, 80, 90, 95 and 100% ethanol. The final step with 100% ethanol was repeated twice. Samples were submerged for 30 minutes in each ethanol-DI mixture. For dehydration, the samples were immersed in increasing concentrations of hexamethyldisilazane (HMDS)-ethanol mixtures in a fume hood; 33.3, 66.6 and 100% HMDS (Sigma, #440191) respectively. Samples were immersed in each HMDS-ethanol mixture for 40 minutes. The final step involving 100% HMDS was repeated twice, and then samples were left submerged in 100% HMDS overnight in a fume hood until completely dry the following day. Dried samples

were gold plated before imaging with Evo LS 15 (Zeiss, Germany) scanning electron microscope.

Immunofluorescence (IF) staining

For 2D protein screening experiments, culture media was aspirated, and cells were washed twice with phosphate buffer saline (PBS; Sigma, #806552) using volumes of 100µl per well for 96-well plates. Fixation was performed using 4% paraformaldehyde (PFA, Insight Biotechnology, #sc-281692) for 20 minutes at 4°C followed by two further PBS washes. 50µl of blocking solution containing 3% donkey serum (Sigma, #D9663-10ML), 0.1% Triton-X (Sigma, #X100-500ML), 1% BSA (Sigma, #12657), and 95.9% PBS was then added to each well. The plate was left for 30mins at room temperature for permeabilization, and blocking, then aspirated for the addition of the primary antibodies without washing. The list of primary antibodies is listed in Table 1. After two hours at room temperature, the primary antibodies were aspirated, and cells were washed twice with 100µl/well PBS in each wash. 50µl/well of secondary antibodies were then added and samples were left to incubate at room temperature in the dark for two hours. The list of secondary antibodies is listed in Table 2. After two hours, secondary antibodies were aspirated, and cells were washed twice with PBS (100µl/well) followed by the addition of DAPI solution (NucBlue™ Fixed, Life Technologies #R37606). Imaging was then performed within 24 hours.

For 3D cardiac and hepatic experiments, cell-laden hydrogel domes first underwent two fifteen-minute washes with PBS (1ml/well for a 24-well place). Samples were then fixed for 60 minutes at 4°C with 4% paraformaldehyde (1ml/well) followed by three 15-minute washes with PBS (1ml/well). Subsequently, cells were permeabilized and blocked in 1% (w/v) bovine serum (Sigma, #A9418), 3% donkey serum (Sigma, #D9663), and 0.1% Triton X-100 (Sigma, #X100) in sterile PBS for one hour at room temperature. The blocking solution was then aspirated, and primary antibodies (1ml/well) were added without any washing. Samples were left overnight at 4°C to incubate. The following day, primary antibodies were aspirated, and samples underwent two fifteen-minute PBS washes. Next, secondary antibodies were added, and samples were left in the dark at room temperature to incubate for three or more hours. Thereafter, the DAPI solution was added and images were acquired at least 30 minutes after the addition of the DAPI solution. For 3D neural experiments, hydrogels

were fixed in 4% PFA for 45 minutes at room temperature then transferred into a 30% w/v sucrose solution (Sigma Aldrich, #S0389) and left for 24 hours. Sucrose-saturated samples were subsequently placed in OCT (ThermoFisher, #23-730-571) and stored at -20ºC. These frozen blocks were then cut into 12µm sections and mounted on coated slides (ThermoFisher, #J1800AMNZ). Sections were then blocked and permeabilised in a 0.3% Triton-X solution containing 10% normal goat serum at room temperature for an hour. Primary antibodies diluted in 0.1% Triton-X containing 5% normal goat serum were then added and incubated overnight at 4ºC. The following day, sections were washed with PBS and secondary antibodies were added and left for an hour at room temperature. Lastly, samples were incubated in DAPI solution for 15 minutes and then mounted using FluorSave (VWR, #345789).

Table 1: List of primary antibodies.

Primary Antibodies (species raised in)	***Vendor***	***Catalogue no.***	***Dilution factor***
OCT4 (rabbit)	ThermoFisher	710788	1:250
NANOG (rabbit)	Abcam	ab109250	1:100
SOX2 (rabbit)	ThermoFisher	PA1-094	1:100
SOX2 (goat)	RnD Systems	AF2018	10 µg/ml
Albumin (goat)	Bethyl	A80-129A	1:100
CD147 (mouse)	Abcam	Ab666	1:100
HNF1A (rabbit)	Cell Signalling	D7Z2Q	1:400
HNF4A (rabbit)	ThermoFisher	MA5-14891	1:2000
Cyp2A6 (chicken)	University of Eastern Finland	Collaborator	1:200
E-cadherin (mouse)	Santa Cruz	SC-31021	1:100
Troponin-T (goat)	Abcam	ab64623	1:100
Smooth Muscle α-Actin (mouse)	Dako	M0851	1:100
Nestin (mouse)	Sigma	N5413-100UG	1:500
B-catenin (rabbit)	ThermoFisher	14-2567-82	1:250

Table 2: List of secondary antibodies.

Secondary Antibodies	***Vendor***	***Catalogue no.***
AlexaFluor 488 donkey anti-goat	ThermoFisher	A11055
AlexaFluor 488 donkey anti-rabbit	Abcam	ab150073
AlexaFlour 488 donkey anti-rabbit	ThermoFisher	A21206
AlexaFluor 564 donkey anti-mouse	ThermoFisher	A10037
AlexaFluor 647 donkey anti-rabbit	Abcam	ab150075
AlexaFluor 647 donkey anti-mouse	ThermoFisher	A32795
AlexaFluor 647 donkey anti-mouse	ThermoFisher	A31571

For IF staining of tissue sections, glass slides with paraffin-embedded sections were rehydrated in xylene (5 minutes x3), then transferred to reducing concentrations of ethanol (100% for 5 minutes x2, 90% for 2 minutes, and 70% for 2 minutes). Thereafter, slides were washed in distilled water for 5 minutes and transferred to pH 6.0 antigen retrieval buffer and heated to 121°C for 15 minutes. After cooling, the slides were re-washed with distilled water. A hydrophobic pen was used to mark the area of interest. Then, TrueBlack® (Biotium, #23007) dissolved in 70% ethanol (1X) was added to the samples for 30 seconds to reduce autofluorescence. Subsequently, slides were rinsed with distilled water and blocking solution, as described above, was added and the samples were left for 30 minutes at room temperature. After 30 minutes, the blocking solution was discarded without washing the samples and goat anti-human albumin primary antibody dissolved in sterile PBS to a final concentration of 1:100 ((as described above) was added to the samples. Slides were then left to incubate at 4°C overnight. The following day, the slides were washed with distilled water, and then 1:200 Alexa Fluor 647 donkey anti-goat secondary antibody (as above) was added. The slides were left for one hour to incubate in the dark at room temperature and then washed again before adding Fluoroshield™ mounting media containing DAPI (Sigma, #F6057). Lastly, coverslips were placed and sealed with nail polish.

Imaging

2D IF and brightfield images of hPSCs were acquired using the Opera Phenix HCHT screening system (PerkinElmer, USA). Optimal acquisition settings were determined as 100ms exposure time and 90% excitation strength; these were kept constant during screening. 3D images of cardiac and hepatic cells and tissue were captured using an LSM710 (Zeiss, Germany) laser scanning confocal microscope at x10 and x20 objectives with corresponding filters. Bright-field images were acquired using an Axio-Obsorber.Z1 (Zeiss, Germany) fluorescence microscope. Images of CDFDA uptake and excretion in iHeps were acquired using an SP-DM8 (Leica, Germany) microscope. 3D images of neuronal cells were acquired using a DM 6000 B (Leica, Germany) microscope.

Young's modulus measurements

Fibrin-only and FLGs were examined under compression using a "see-saw" method that was previously described (68). Briefly, a central pivot on a frictionless support base evenly balanced two arms of a rod. On one arm a flat loading platen was attached, and the load was increased at a constant rate (~1.67×10^{-4} $N \cdot s^{-1}$) by the addition of aluminium weights. Displacements were then measured with a bi-axial laser micrometre (resolution of ±3 µm). From the tangent slope of the stress-strain curves (up to 5% strain), the through-thickness Young's modulus was calculated (n=5 in each group).

Gene expression analyses by quantitative polymerase chain reaction (qPCR)

Ribonucleic acid (RNA) was extracted using TriZOL™ (ThermoFisher, #15596026) and purified using the Direct-zol RNA Miniprep Kit (Zymo Research, #R2050-R2053). cDNA was made using Superscript Reverse Transcriptase IV (ThermoFisher, #18090010) following the manufacturer's protocol. Quantitative PCR was run on Quantstudio 5 (ThermoFisher, #A34322I) using the KAPA SYBR FAST qPCR kit (Roche, #KK4601). Data were analysed using the 2^(ΔΔCt) method. Sequences of the primer pairs are listed in Table 3.

Table 5.3: Sequences for forward and reverse primers used.

Target gene	***Forward primer sequence***	***Reverse primer sequence***

ABCC2	TTCGTTCCAGACGCAGTCCAGG	CCAGGAGCCATAGGTAGCCCAA
APOB	TGTTAGGACACCAGCCCTCCA	GCCCGAAGGCTGAAATGGTCT
AFP	AACTATTGGCCTGTGGCGAGG	TGAAGCATGGCCTCCTGTTGG
BAAT	TGTGCCTCAACGACCCACGAT	GGGGGAGACATTCCGCCATGAA
CEBPA	AAGTCGGTGGACAAGAACAGCAA	TTGTCACTGGTCAGCTCCAGCA
CYP27A1	GCTGTTCGTTCAAGGCTATGCCC	ACTGGGTACTTGCCCTCTTGCC
CYP3A4	TGTGCCTGAGAACACCAGAG	GTGGTGGAAATAGTCCCGTG
CYP3A5	ACAAGACCCCTTTGTGGAGAGC	TTGTTTGTCGTTGAGGCGACTT
CYP3A7	TGGACCCAGAAACTGCATTGGC	ATCAGGCTCCACTTACGGTCTCA
CK7	AAGCAGGATATGGCACGGCAG	CACTCCATCTCCAGCCAACCG
CK19	GGCGATGTGCGAGCTGATAGT	CGGTAGGTGGCAATCTCCTGC
FOXA1	CCTTCAACCACCCGTTCTCCA	CGGGCAACGTAGAGCCGTAAG
FOXA2	GCCTACGAACAGGTGATGCACTA	CAGGCCCGTTTTGTTCGTGAC
GATA6	AGCACCAATCCCGAGAACAGC	GTCGCACGGAGGACGTGACTT
GATA4	TCCATCCACCCTGTCCTCTCG	GCTTGGAGCTGGTCTGTGGAG
G6PC	TACAGCAACACTTCCGTGCCCC	GCACAGCCCAGAATCCCAACCA
GGT	ACAACCAGCTTCTGCCCAACG	GACGCGATCTGGGTGTGATGG
HNF4A	GAGATGCTGCTGGGAGGGTCC	GGGTCTCAGGGGTGGACATCT
LGR5	CCTGCTTGATGGCTGGCTGAT	CACTGCTGCGATGACCCCAAT
PDK4	TACAGCAACACTTCCGTGCCCC	GCACAGCCCAGAATCCCAACCA
SOX9	CAACAGATCGCCTACAGCCCC	CGTACTGTGAGCGGGTGATGG
TAT	TGGAAACCTGCCTACAGACC	TAGCTTCTAGGGGTGCCTCA
TF	CCGATGGTCCCAGTGTTGCTT	AACTCTGCCACCACAGGCTTC
TBX3	GGGACACTGGAAATGGCCGAA	GGAGAAGAAGCCTGGGCGAAG
MUC2	GCTGACGAGTGGTTGGTGAATG	GATGAGGTGGCAGACAGGAGAC

Enzyme-linked immunosorbent assays (ELISA)

Laminin concentrations in supernatants were measured using a laminin ELISA kit (Insight Biotechnology, #Boster Pikokine™ EK0434). Acellular FLGs and fibrin gels were synthesized, and sterile DMEM/F12 media was added 30mins after gelation. Media was collected the next day (Day 1) and then every other day for two weeks. Supernatants were stored at -20ºC until they were analysed alongside stock concentrations of laminin for comparison using the Laminin ELISA kit as per the manufacturer's instructions. Sample absorbance readings were then taken using a FLUOstar® Omega plate reader (BMG Labtech Ltd, UK) at 450 nm. The residual amount of laminin in FLGs was estimated by the following equation:

$$1 - \frac{Total\ Laminin\ 521\ in\ supernatant\ after\ hydrogel\ gelation\ (weight)}{Measured\ Laminin\ 521\ in\ stock\ solution\ added\ to\ the\ hydrogel\ (weight)}$$

Albumin concentrations in supernatants were measured using a human albumin ELISA quantification kit (Bethyl Lab, #E80-129). Sample absorbance was measured with a Synergy HTX microplate reader (BioTek, USA). Supernatants from PHH hepatocytes were collected 24 hours after the completion of cell recovery. Supernatants from iHeps were collected 2 days after (Day 22) the end of the differentiation protocol (Day 20); media was refreshed every other day as per differential protocol).

APOB secretion in the supernatant was quantified using the human APOB ELISA quantification kit (Mabtech, # 3715-1H-6) according to product literature. Sample absorbance was measured with an Infinite M1000 PRO microplate reader (Tecan, Switzerland). Supernatants from iHeps were collected 2 days after (Day 22) the end of the differentiation protocol (Day 20); media was refreshed every other day as per differential protocol).

Cytochrome 3A4 (CYP3A4) assay

CYP3A4 activity was measured using the P450-Glo^{TM} CYP3A4 Assay kit (Promega, #V9001) as per the manufacturer's protocol. Fluorescence in samples was measured using the Synergy HTX microplate reader. PHH after 24 hours of cell recovery and Day 22 iHeps were used.

Low-density Lipoprotein (LDL) uptake cell-based assay

LDL uptake was demonstrated using a cell-based kit (Cayman chem, #10011125) following the manufacturer's protocol. iHeps were incubated for 12 hours, then the HCM media was replaced with PBS. Images were then acquired immediately. Day 22 iHeps and hPSCs (negative control) were used.

5-(and-6)-Carboxy-2',7'-Dichlorofluorescein Diacetate (6-CDF)

6-CDF was used to demonstrate hepatocyte function following a protocol previously described (31). 3D iHeps (Day 22) were incubated for 2 hours with HCM media containing 1µmol/L of 6-CDF (Thermofisher, #C-369). Samples were then washed with PBS for 15 minutes before staining with Hoescht in HCM.

Gamma-glutamyl Transfer (GGT) assay

GGT activity was determined by a fluorometric GGT assay kit (Abcam, #ab241030) as per product literature. Fluorescence in samples was measured with the Infinite M1000 PRO microplate reader. PHH after 24 hours of cell recovery and Day 22 iHeps were used. PHH after 24 hours of cell recovery and Day 22 iHeps were used.

Animal experimentation

Biocompatibility studies were performed in immunocompetent general-purpose C57BL/6 ("Black 6") mice obtained from InVivos (www.invivos.com.sg). Only healthy, normal strain male mice between two to three months old (~ 30g to 35g) were used. 100% croton oil (Merck, #C6719-10G) was emulsified in corn oil to a final concentration of 1.0% *v/v, referred to herein as "croton oil".* Croton oil was used as a positive control because it is a well-known skin allergen that is commonly used to study inflammation in murine models (69). 200µl of croton oil (n=9), Alphagel (n=9), fibrin-only gel (n=9), and 0.9% saline (n=9) was injected subcutaneously using 18G hypodermic needles and 1ml low dead volume syringes into the flanks or scruffed backs of Black 6 mice with aseptic techniques. These volumes were within internationally recommended limits for subcutaneous murine injections (American Association for Laboratory Animal Science). Three mice from each group were culled at 1 week, 2 weeks, and 6 weeks post-injection. Mice were culled by cervical dislocation under general anaesthesia with isofluorane. Injection sites were excised and fixed in 10% formalin for 24 hours then transferred into 70% ethanol. Tissues were then embedded in liquid paraffin, sectioned by microtome, and placed on glass slides. Slides were stained for hematoxylin and eosin (H&E) to allow for evaluation for signs of inflammation, then imaged with the TissueFAXS i-plus system (TissueGnostics, Vienna, Austria).

For the intrahepatic injections of iHeps, NSG™ mice (also known as NOD SCID gamma or NSG NOD.Cg-*Prkdcscid Il2rgtm1Wjl*/SzJ mice) from InVivos (www.invivos.com.sg) were acquired and bred in-house by the Dan Yock Young (DYY) lab in the CeLS Vivarium, National University of Singapore. Both male and female mice were used. All mice were between four to five months old and weight ~ 40g to 50g. All mice were anaesthetised with isoflurane and had their abdomen shaved pre-operatively. Surgical laparotomies were then performed aseptically to reveal the lower

liver margin for injections. For H-iHep transplantations, 3 x 10^6 million freshly harvested Day 22 H-iHeps were harvested and re-suspended in 75µl of either Hepatogel (n=9) or sterile 0.9% saline (n=9), then injected under direct vision with a 1ml low dead volume syringe and 18G hypodermic needle into the inferior margins of the right liver lobe. All mice were given prophylactic antibiotics and analgesia subcutaneously for three days after the operation. 3 mice from each group were culled on Day 3, Day 7-, and 2 months post-hepatocyte transplantation.

All mice were fed rodent maintenance food (#2918 Teklad Irradiated Global, 18% Protein rodent diet, Envigo, Hackensack, NJ) and kept on bedding from BioCOB. Approval for all animal work was granted by the National University of Singapore Institutional Animal Care and Use Committee (IACUC), protocol number R20-0822.

Statistical analyses

Prism 9.3.0 (GraphPad, USA) was used for data analyses and the generation of bar graphs. Data were tested for normal distribution using the Shapiro-Wilk method. Parametric data and their bar charts were presented as mean and standard deviation unless otherwise stated. For comparison between two groups of values, the student's t-test was used to compare means for parametric values; the Chi-squared test or Mann-Whitney U test was used to test for associations in non-parametric values. When more than two groups were compared, one-way analysis of variance (ANOVA) with Tukey correction was performed on parametric data; the Kruskal-Wallis test was used when data were not parametric All tests were two-sided, and the alpha was set at 5%.

References

1. Hofer M, Lutolf MP. Engineering organoids. Nat Rev Mater. 2021 May;6(5):402–20.
2. Pampaloni F, Reynaud EG, Stelzer EHK. The third dimension bridges the gap between cell culture and live tissue. Nat Rev Mol Cell Biol. 2007 Oct;8(10):839–45.
3. Gjorevski N, Nikolaev M, Brown TE, Mitrofanova O, Brandenberg N, DelRio FW, et al. Tissue geometry drives deterministic organoid patterning. Science. 2022 Jan 7;375(6576):eaaw9021.
4. Aisenbrey EA, Murphy WL. Synthetic alternatives to Matrigel. Nat Rev Mater. 2020 Jul;5(7):539–51.

878 5. Baker M. Stem cells in culture: defining the substrate. Nat Methods. 2011 Apr;8(4):293–7.

879 6. Vukicevic S, Kleinman HK, Luyten FP, Roberts AB, Roche NS, Reddi AH. Identification of multiple
880 active growth factors in basement membrane Matrigel suggests caution in interpretation of
881 cellular activity related to extracellular matrix components. Exp Cell Res. 1992 Sep;202(1):1–8.

882 7. Soofi SS, Last JA, Liliensiek SJ, Nealey PF, Murphy CJ. The elastic modulus of Matrigel as
883 determined by atomic force microscopy. J Struct Biol. 2009 Sep;167(3):216–9.

884 8. Hughes CS, Postovit LM, Lajoie GA. Matrigel: a complex protein mixture required for optimal
885 growth of cell culture. Proteomics. 2010 May;10(9):1886–90.

886 9. Passaniti A, Kleinman HK, Martin GR. Matrigel: history/background, uses, and future applications.
887 J Cell Commun Signal. 2022 Dec;16(4):621–6.

888 10. Liu H, Bockhorn J, Dalton R, Chang YF, Qian D, Zitzow LA, et al. Removal of lactate
889 dehydrogenase-elevating virus from human-in-mouse breast tumor xenografts by cell-sorting. J
890 Virol Methods. 2011 May;173(2):266–70.

891 11. Farhat W, Hasan A, Lucia L, Becquart F, Ayoub A, Kobeissy F. Hydrogels for Advanced Stem
892 Cell Therapies: A Biomimetic Materials Approach for Enhancing Natural Tissue Function. IEEE Rev
893 Biomed Eng. 2019;12:333–51.

894 12. Cruz-Acuña R, Quirós M, Huang S, Siuda D, Spence JR, Nusrat A, et al. PEG-4MAL hydrogels
895 for human organoid generation, culture, and in vivo delivery. Nat Protoc. 2018 Sep;13(9):2102–
896 19.

897 13. Labouesse C, Tan BX, Agley CC, Hofer M, Winkel AK, Stirparo GG, et al. StemBond hydrogels
898 control the mechanical microenvironment for pluripotent stem cells. Nat Commun. 2021 Oct
899 21;12(1):6132.

900 14. Yin S, Cao Y. Hydrogels for Large-Scale Expansion of Stem Cells. Acta Biomater. 2021 Jul
901 1;128:1–20.

902 15. Wang X, Rivera-Bolanos N, Jiang B, Ameer GA. Advanced Functional Biomaterials for Stem
903 Cell Delivery in Regenerative Engineering and Medicine. Adv Funct Mater. 2019;29(23):1809009.

904 16. Broguiere N, Isenmann L, Hirt C, Ringel T, Placzek S, Cavalli E, et al. Growth of Epithelial
905 Organoids in a Defined Hydrogel. Adv Mater. 2018;30(43):1801621.

906 17. Ye S, Boeter JWB, Mihajlovic M, van Steenbeek FG, van Wolferen ME, Oosterhoff LA, et al. A
907 Chemically Defined Hydrogel for Human Liver Organoid Culture. Adv Funct Mater.
908 2020;30(48):2000893.

909 18. Domogatskaya A, Rodin S, Boutaud A, Tryggvason K. Laminin-511 but Not -332, -111, or -411
910 Enables Mouse Embryonic Stem Cell Self-Renewal In Vitro. STEM CELLS. 2008;26(11):2800–9.

911 19. Horejs CM, Serio A, Purvis A, Gormley AJ, Bertazzo S, Poliniewicz A, et al. Biologically-active
912 laminin-111 fragment that modulates the epithelial-to-mesenchymal transition in embryonic
913 stem cells. Proc Natl Acad Sci U S A. 2014 Apr 22;111(16):5908–13.

914 20. Li L, Arman E, Ekblom P, Edgar D, Murray P, Lonai P. Distinct GATA6- and laminin-dependent
915 mechanisms regulate endodermal and ectodermal embryonic stem cell fates. Dev Camb Engl.
916 2004 Nov;131(21):5277–86.

917 21. Ong J, Serra MP, Segal J, Cujba AM, Ng SS, Butler R, et al. Imaging-Based Screen Identifies
918 Laminin 411 as a Physiologically Relevant Niche Factor with Importance for i-Hep Applications.
919 Stem Cell Rep. 2018 Mar 13;10(3):693–702.

920 22. Ong J, Zhao J, Levy GK, Macdonald J, Justin AW, Markaki AE. Functionalisation of a heat-
921 derived and bio-inert albumin hydrogel with extracellular matrix by air plasma treatment. Sci Rep.
922 2020 Jul 24;10(1):12429.

923 23. Borowski M, Giovino-Doherty M, Ji L, Shi MJ, Smith KP. Basic pluripotent stem cell culture
924 protocols. In: Laning J, editor. StemBook [Internet]. Cambridge (MA): Harvard Stem Cell Institute;
925 2008 [cited 2023 May 13]. Available from: http://www.ncbi.nlm.nih.gov/books/NBK133258/

926 24. Stem Cell Culture Guide [Internet]. [cited 2023 May 13]. Available from:
927 https://www.atcc.org/resources/culture-guides/stem-cell-culture-guide

928 25. Goetzke R, Keijdener H, Franzen J, Ostrowska A, Nüchtern S, Mela P, et al. Differentiation of
929 Induced Pluripotent Stem Cells towards Mesenchymal Stromal Cells is Hampered by Culture in 3D
930 Hydrogels. Sci Rep. 2019 Oct 30;9(1):15578.

931 26. Jones M, Gabriel DA. Influence of the subendothelial basement membrane components on
932 fibrin assembly. Evidence for a fibrin binding site on type IV collagen. J Biol Chem. 1988 May
933 25;263(15):7043–8.

934 27. Marcinczyk M, Elmashhady H, Talovic M, Dunn A, Bugis F, Garg K. Laminin-111 enriched
935 fibrin hydrogels for skeletal muscle regeneration. Biomaterials. 2017 Oct;141:233–42.

936 28. Woodcock-Mitchell J, Mitchell JJ, Low RB, Kieny M, Sengel P, Rubbia L, et al. Alpha-smooth
937 muscle actin is transiently expressed in embryonic rat cardiac and skeletal muscles. Differ Res Biol
938 Divers. 1988 Dec;39(3):161–6.

939 29. Maroof AM, Keros S, Tyson JA, Ying SW, Ganat YM, Merkle FT, et al. Directed differentiation
940 and functional maturation of cortical interneurons from human embryonic stem cells. Cell Stem
941 Cell. 2013 May 2;12(5):559–72.

942 30. Chambers SM, Fasano CA, Papapetrou EP, Tomishima M, Sadelain M, Studer L. Highly
943 efficient neural conversion of human ES and iPS cells by dual inhibition of SMAD signaling. Nat
944 Biotechnol. 2009 Mar;27(3):275–80.

945 31. Ramli MNB, Lim YS, Koe CT, Demircioglu D, Tng W, Gonzales KAU, et al. Human Pluripotent
946 Stem Cell-Derived Organoids as Models of Liver Disease. Gastroenterology. 2020
947 Oct;159(4):1471-1486.e12.

948 32. Ang LT, Tan AKY, Autio MI, Goh SH, Choo SH, Lee KL, et al. A Roadmap for Human Liver
949 Differentiation from Pluripotent Stem Cells. Cell Rep. 2018 Feb;22(8):2190–205.

950 33. Schafer KA, Eighmy J, Fikes JD, Halpern WG, Hukkanen RR, Long GG, et al. Use of Severity
951 Grades to Characterize Histopathologic Changes. Toxicol Pathol. 2018 Apr;46(3):256–65.

952 34. Thuilliez C, Dorso L, Howroyd P, Gould S, Chanut F, Burnett R. Histopathological lesions
953 following intramuscular administration of saline in laboratory rodents and rabbits. Exp Toxicol
954 Pathol Off J Ges Toxikol Pathol. 2009 Jan;61(1):13–21.

955 35. National Toxicology Program [Internet]. [cited 2023 May 24]. Nonneoplastic Lesion Atlas.
956 Available from: https://ntp.niehs.nih.gov/atlas/nnl

957 36. Avior Y, Sagi I, Benvenisty N. Pluripotent stem cells in disease modelling and drug discovery.
958 Nat Rev Mol Cell Biol. 2016 Mar;17(3):170–82.

959 37. Hannan NRF, Segeritz CP, Touboul T, Vallier L. Production of hepatocyte like cells from
960 human pluripotent stem cells. Nat Protoc. 2013 Feb;8(2):430–7.

961 38. Klaffky E, Williams R, Yao CC, Ziober B, Kramer R, Sutherland A. Trophoblast-specific
962 expression and function of the integrin alpha 7 subunit in the peri-implantation mouse embryo.
963 Dev Biol. 2001 Nov 1;239(1):161–75.

964 39. Pook M, Teino I, Kallas A, Maimets T, Ingerpuu S, Jaks V. Changes in Laminin Expression
965 Pattern during Early Differentiation of Human Embryonic Stem Cells. PloS One.
966 2015;10(9):e0138346.

967 40. Galanakis D, Nuovo G, Spitzer S, Kaplan C, Scharrer I. Fibrinogen mRNA and antigen co-
968 present in human trophoblasts in situ: possible implications. Thromb Res. 1996 Jan 15;81(2):263–
969 9.

970 41. Weisel JW, Litvinov RI. Fibrin Formation, Structure and Properties. Subcell Biochem.
971 2017;82:405–56.

972 42. Sánchez-Cortés J, Mrksich M. The platelet integrin alphaIIbbeta3 binds to the RGD and AGD
973 motifs in fibrinogen. Chem Biol. 2009 Sep 25;16(9):990–1000.

974 43. Suehiro K, Mizuguchi J, Nishiyama K, Iwanaga S, Farrell DH, Ohtaki S. Fibrinogen binds to
975 integrin alpha(5)beta(1) via the carboxyl-terminal RGD site of the Aalpha-chain. J Biochem
976 (Tokyo). 2000 Oct;128(4):705–10.

977 44. Wondimu Z, Omrani S, Ishikawa T, Javed F, Oikawa Y, Virtanen I, et al. A Novel Monoclonal
978 Antibody to Human Laminin α5 Chain Strongly Inhibits Integrin-Mediated Cell Adhesion and
979 Migration on Laminins 511 and 521. PLOS ONE. 2013 Jan 7;8(1):e53648.

980 45. Ishihara J, Ishihara A, Fukunaga K, Sasaki K, White MJV, Briquez PS, et al. Laminin heparin-
981 binding peptides bind to several growth factors and enhance diabetic wound healing. Nat
982 Commun. 2018 Jun 4;9(1):2163.

983 46. Gandhi JK, Knudsen T, Hill M, Roy B, Bachman L, Pfannkoch-Andrews C, et al. Human
984 Fibrinogen for Maintenance and Differentiation of Induced Pluripotent Stem Cells in Two
985 Dimensions and Three Dimensions. Stem Cells Transl Med. 2019 Feb 15;8(6):512–21.

986 47. Frye M, Taddei A, Dierkes C, Martinez-Corral I, Fielden M, Ortsäter H, et al. Matrix stiffness
987 controls lymphatic vessel formation through regulation of a GATA2-dependent transcriptional
988 program. Nat Commun. 2018 Apr 17;9(1):1511.

989 48. Garcia-Abrego C, Zaunz S, Toprakhisar B, Subramani R, Deschaume O, Jooken S, et al.
990 Towards Mimicking the Fetal Liver Niche: The Influence of Elasticity and Oxygen Tension on

991 Hematopoietic Stem/Progenitor Cells Cultured in 3D Fibrin Hydrogels. Int J Mol Sci. 2020
992 Jan;21(17):6367.

993 49. Chowdhury F, Li Y, Poh YC, Yokohama-Tamaki T, Wang N, Tanaka TS. Soft substrates
994 promote homogeneous self-renewal of embryonic stem cells via downregulating cell-matrix
995 tractions. PloS One. 2010 Dec 13;5(12):e15655.

996 50. Liu J, Tan Y, Zhang H, Zhang Y, Xu P, Chen J, et al. Soft fibrin gels promote selection and
997 growth of tumourigenic cells. Nat Mater. 2012 Jul 1;11(8):734–41.

998 51. Genovese P, Patel A, Ziemkiewicz N, Paoli A, Bruns J, Case N, et al. Co-delivery of fibrin-
999 laminin hydrogel with mesenchymal stem cell spheroids supports skeletal muscle regeneration
1000 following trauma. J Tissue Eng Regen Med. 2021;15(12):1131–43.

1001 52. Ziemkiewicz N, Hilliard GM, Dunn AJ, Madsen J, Haas G, Au J, et al. Laminin-111-Enriched
1002 Fibrin Hydrogels Enhance Functional Muscle Regeneration Following Trauma. Tissue Eng Part A.
1003 2022 Apr;28(7–8):297–311.

1004 53. Nam K, Maruyama CL, Wang CS, Trump BG, Lei P, Andreadis ST, et al. Laminin-111-derived
1005 peptide conjugated fibrin hydrogel restores salivary gland function. PLOS ONE. 2017 Nov
1006 2;12(11):e0187069.

1007 54. Huch M, Boj SF, Clevers H. Lgr5(+) liver stem cells, hepatic organoids and regenerative
1008 medicine. Regen Med. 2013 Jul;8(4):385–7.

1009 55. Jha R, Xu RH, Xu C. Efficient Differentiation of Cardiomyocytes from Human Pluripotent Stem
1010 Cells with Growth Factors. Methods Mol Biol Clifton NJ. 2015;1299:115–31.

1011 56. Rhee YH, Puspita L, Sulistio YA, Kim SW, Vidyawan V, Elvira R, et al. Efficient Neural
1012 Differentiation of hPSCs by Extrinsic Signals Derived from Co-cultured Neural Stem or Precursor
1013 Cells. Mol Ther. 2019 Jul 3;27(7):1299–312.

1014 57. Lancaster MA, Corsini NS, Wolfinger S, Gustafson EH, Phillips AW, Burkard TR, et al. Guided
1015 self-organization and cortical plate formation in human brain organoids. Nat Biotechnol. 2017
1016 Jul;35(7):659–66.

1017 58. Dhawan A, Puppi J, Hughes RD, Mitry RR. Human hepatocyte transplantation: current
1018 experience and future challenges. Nat Rev Gastroenterol Hepatol. 2010 May;7(5):288–98.

1019 59. Forbes SJ, Gupta S, Dhawan A. Cell therapy for liver disease: From liver transplantation to
1020 cell factory. J Hepatol. 2015 Apr;62(1 Suppl):S157-169.

1021 60. Dhawan A, Chaijitraruch N, Fitzpatrick E, Bansal S, Filippi C, Lehec SC, et al. Alginate
1022 microencapsulated human hepatocytes for the treatment of acute liver failure in children. J
1023 Hepatol. 2020 May;72(5):877–84.

1024 61. Zhao T, Zhang ZN, Rong Z, Xu Y. Immunogenicity of induced pluripotent stem cells. Nature.
1025 2011 May 13;474(7350):212–5.

1026 62. Tricot T, Verfaillie CM, Kumar M. Current Status and Challenges of Human Induced
1027 Pluripotent Stem Cell-Derived Liver Models in Drug Discovery. Cells. 2022 Jan;11(3):442.

1028 63. Mallanna SK, Duncan SA. Differentiation of hepatocytes from pluripotent stem cells. Curr
1029 Protoc Stem Cell Biol. 2013 Sep 20;26:1G.4.1-1G.4.13.

1030 64. Cheung C, Bernardo AS, Pedersen RA, Sinha S. Directed differentiation of embryonic origin-
1031 specific vascular smooth muscle subtypes from human pluripotent stem cells. Nat Protoc. 2014
1032 Apr;9(4):929–38.

1033 65. Burridge PW, Holmström A, Wu JC. Chemically Defined Culture and Cardiomyocyte
1034 Differentiation of Human Pluripotent Stem Cells. Curr Protoc Hum Genet. 2015 Oct 6;87:21.3.1-
1035 21.3.15.

1036 66. Tyzack GE, Sitnikov S, Barson D, Adams-Carr KL, Lau NK, Kwok JC, et al. Astrocyte response to
1037 motor neuron injury promotes structural synaptic plasticity via STAT3-regulated TSP-1 expression.
1038 Nat Commun. 2014 Jul 11;5:4294.

1039 67. Katarivas Levy G, Ong J, Birch MA, Justin AW, Markaki AE. Albumin-Enriched Fibrin Hydrogel
1040 Embedded in Active Ferromagnetic Networks Improves Osteoblast Differentiation and Vascular
1041 Self-Organisation. Polymers. 2019 Oct 24;11(11):1743.

1042 68. Varley MC, Neelakantan S, Clyne TW, Dean J, Brooks RA, Markaki AE. Cell structure, stiffness
1043 and permeability of freeze-dried collagen scaffolds in dry and hydrated states. Acta Biomater.
1044 2016 Mar;33:166–75.

1045 69. Kitajima M, Kimura A, Suzuki H. Cutting Edge: Nqo1 Regulates Irritant Contact
1046 Hypersensitivity against Croton Oil through Maintenance of Dendritic Epidermal T Cells. J
1047 Immunol Baltim Md 1950. 2018 Mar 1;200(5):1555–9.

1048

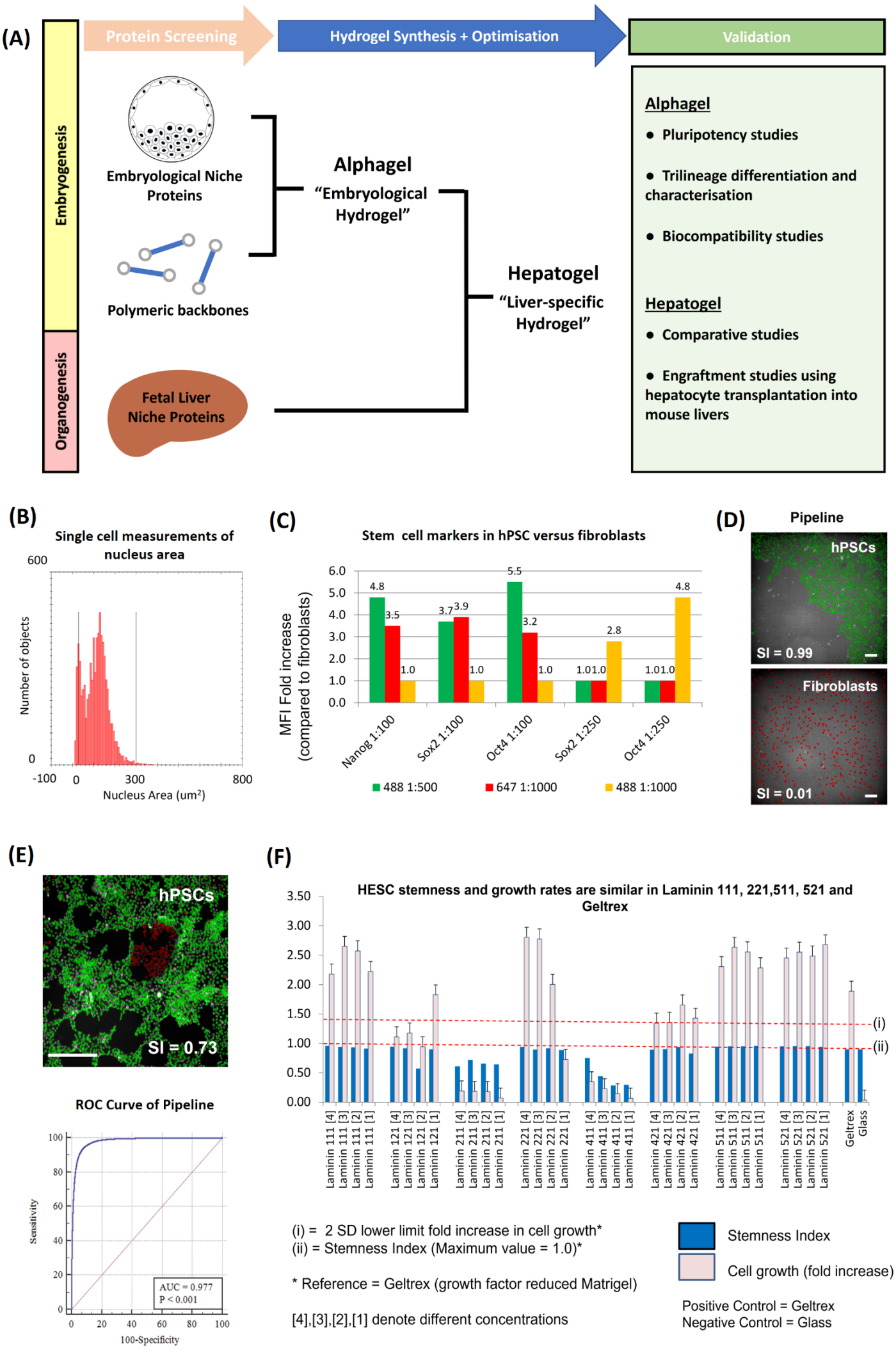

Figure 1. (A) Schematic of workflow. (B) Histogram demonstrating differences in nuclear area in human stem cells. (C) Fold increase in mean fluorescent intensity (MFI) in hPSCs cells compared to fibroblast at various primary and secondary antibody concentrations. (D) Discriminatory potential of the pipeline at discriminating hPSCs from fibroblasts; green = positively identified stem cells (automated) and red = excluded non-stem cells (automated). Scale bar = 200µm. (E) Top panel: Machine learning discriminating undifferentiated hPSCs (green) from spontaneously differentiated hPSCs (red) in extended cell culture (Day 9), scale bar = 200µm. Bottom panel: Receiver operating characteristic (ROC) curve of pipeline. (F) An example of a screening panel. Calculated stemness index (SI) and growth rates of hPSCs on laminins after 1 week in culture (n=3 biological samples with 3 experimental replicates at each concentration).

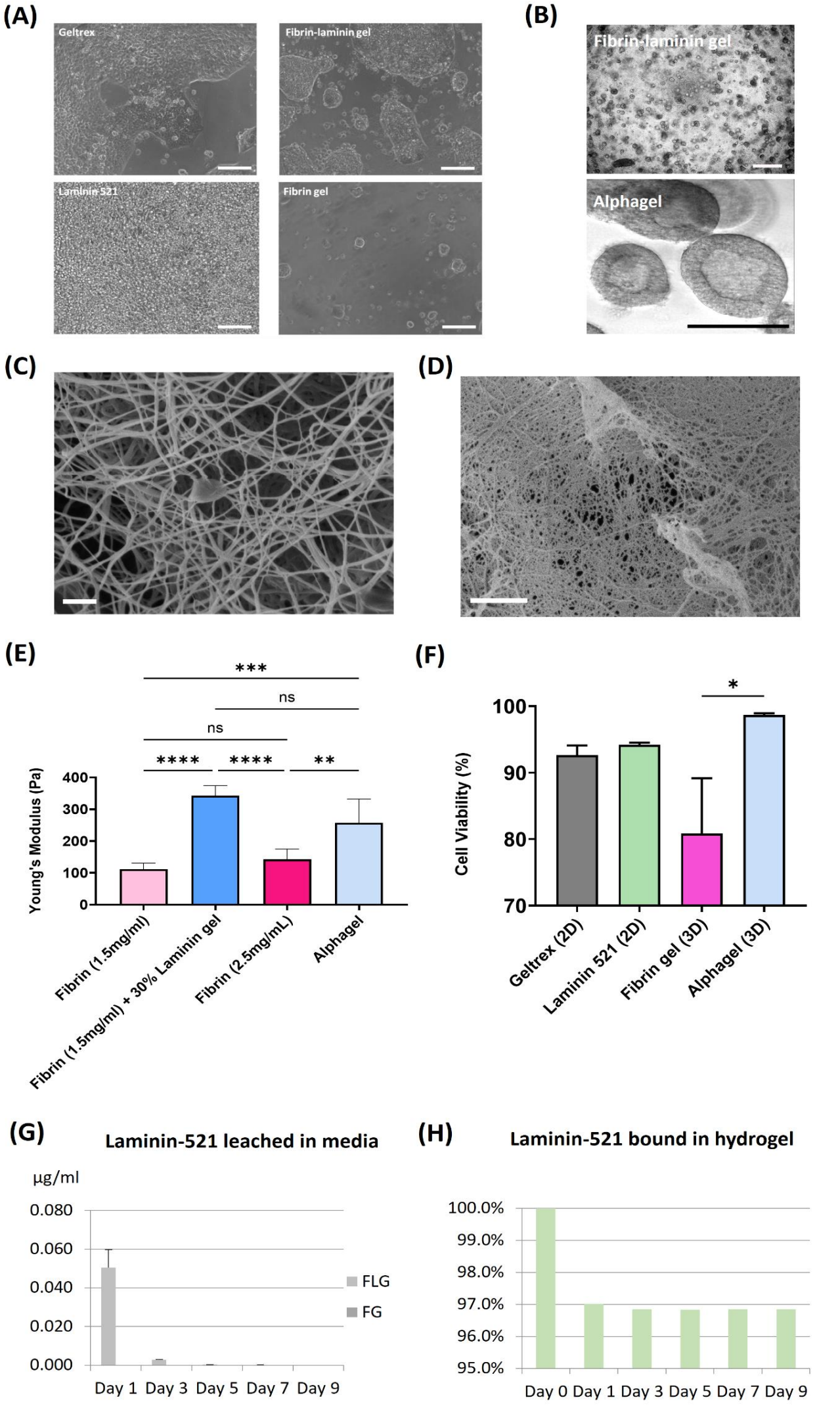

Figure 2. (A) Cell confluence of hPSC cultured in 2D on growth factor reduced Matrigel (Geltrex), Laminin 521, fibrin-laminin hydrogel, and fibrin-only gel after four days. Scale bar = 100µm. (B) hPSCs cultured in 3D hydrogels. Top panel: "High" concentration fibrin (5mg/ml) and "low" Laminin 521 (5µg/ml) concentration. Bottom panel: Alphagel containing structures resembling embryoid bodies, scale bars = 200µm. (C) SEM of fibrin-only hydrogel, scale bar = 1 µm, magnification 20K X, iProbe = 20pA, 6.00kV, WD = 11.0mm. (D) SEM of Alphagel, scale bar = 1 µm, magnification 20K X, iProbe = 13pA, 2.00kV, WD = 4.4mm. (E) Measurements of Young's moduli in hydrogels with varying fibrin and laminin concentrations. One-way ANOVA; ** = $p < 0.01$, *** = $p < 0.001$, and **** = $p < 0.0001$. (F) Cell viability of hPSCs cultured in Alphagel, fibrin-only hydrogels, and 2D standard substrates. Mean ± S.E.M displayed. t-test; * = $p < 0.05$. (G) ELISA of Laminin 521 in culture media used with acellular Alphagel and (H) the calculated amount of fibrin-bound laminin over time.

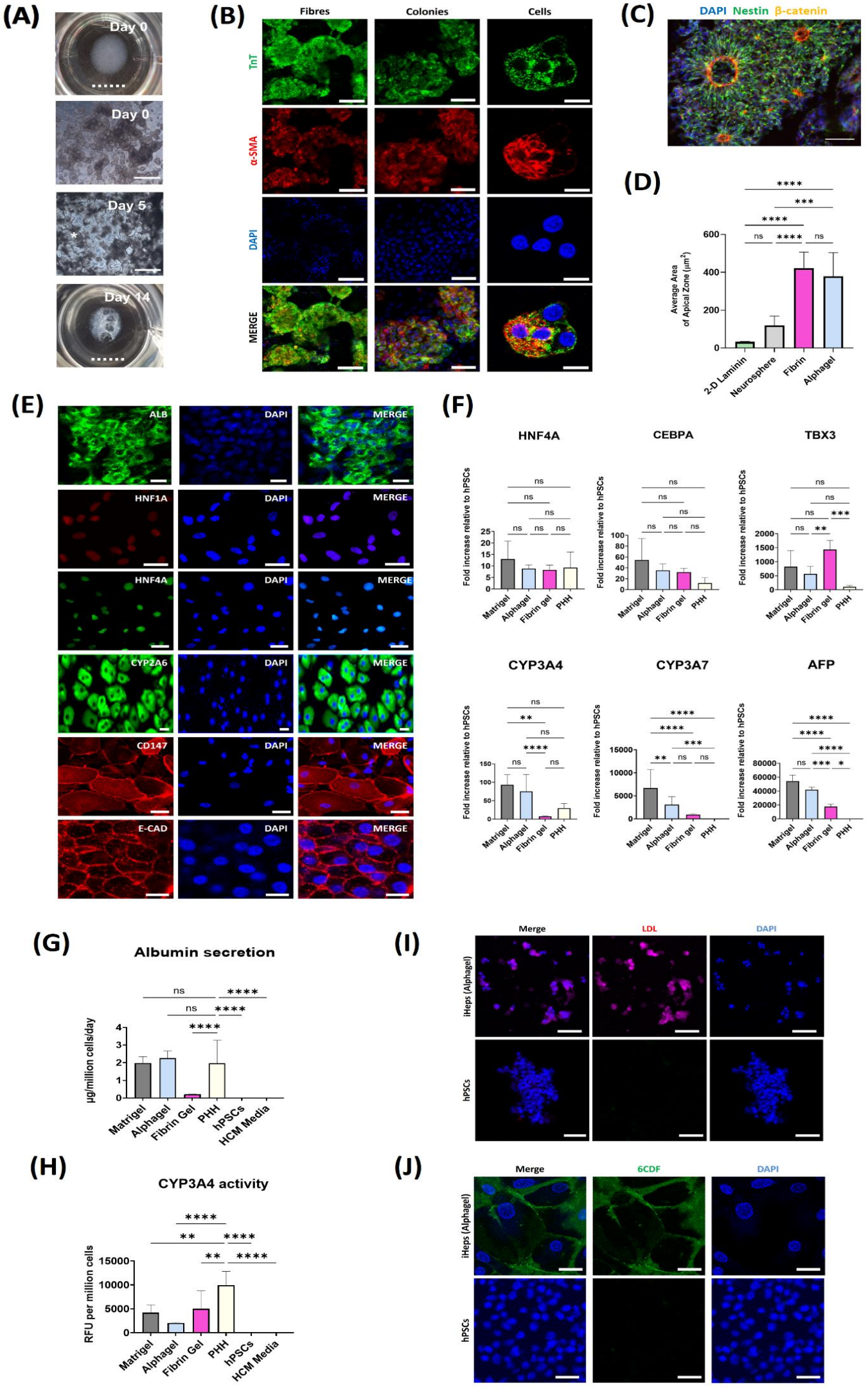

Figure 3: (A) Macroscopic and microscopic appearances of cells in Alphagel. Contractile cardiomyocyte colonies (*) are visible by Day 6. By Day 14 contractile tissue resembling trabeculae carnae is observed. Scale bar: full line = 100μm, dotted line = 1cm. (B) Troponin T (TnT), alpha-smooth muscle actin (α-SMA), and DAPI in cardiomyocytes cultured with Alphagel. Scale bar = 100μm (fibres), 50μm (colonies), and 20μm (cells). (C) Neural progenitors showing Nestin, β catenin, and DAPI staining. Scale bar = 50μm. (D) Average lumen area of neuroepithelia, controls (neurospheres, fibrin-only gel, 2D laminin) vs. Alphagel. (E) Key hepatocyte markers in Alphagel-derived iHeps. ALB = albumin, HNF = Hepatocyte Nuclear Factor, CYP2A6 = Cytochrome 2A6, CD147 = Cluster of Differentiation protein 147, and E-CAD = E-cadherin. Scale bar = 25μm. (F) Key hepatocyte markers by gene expression (qPCR). (G) Albumin secretion (ELISA) and (H) CYP3A4 activity (P450-Glo™) in PHH vs iHeps cultured in various gels (Day 22). HCM = Hepatocyte Culture Media (Lonza). (I) LDL uptake (red) in iHeps cultured in Alphagel. Scale bar = 100μm. (J) CDFDA secretion (green) in iHeps derived in Alphagel. Top panel scale bar = 20μm, bottom panel scale bar = 50μm. For (D), the Kruskal-Wallis test was used for non-parametric data. For all other comparisons, the one-way ANOVA was used. * = $p < 0.05$, ** = $p < 0.01$, *** = $p < 0.001$, and **** = $p < 0.0001$.

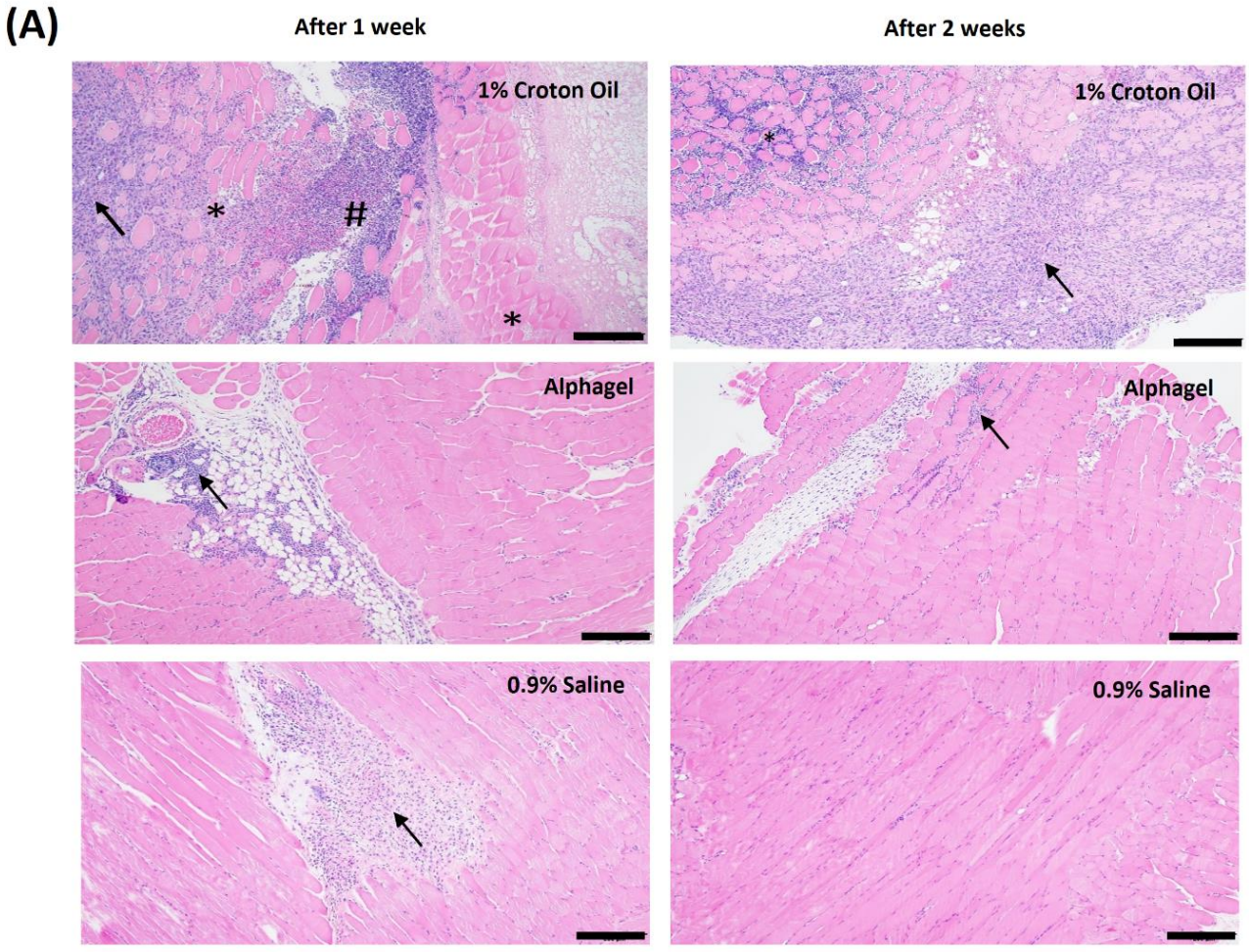

(B)

Inflammation Severity

	Week 1: Grade (Score)	Week 2: Grade (Score)	Weeks 4-6: Grade (Score)
1% Croton oil	Severe (13.3 ± 2.5)	Severe (14.7 ± 4.0)	Culled (N/A)
Alphagel	Mild (4.3 ± 1.5)	Minimal (3.3 ± 0.6)	Normal (0)
0.9% Saline	Minimal (0.25 ± 0.05)	Normal (0)	Normal (0)

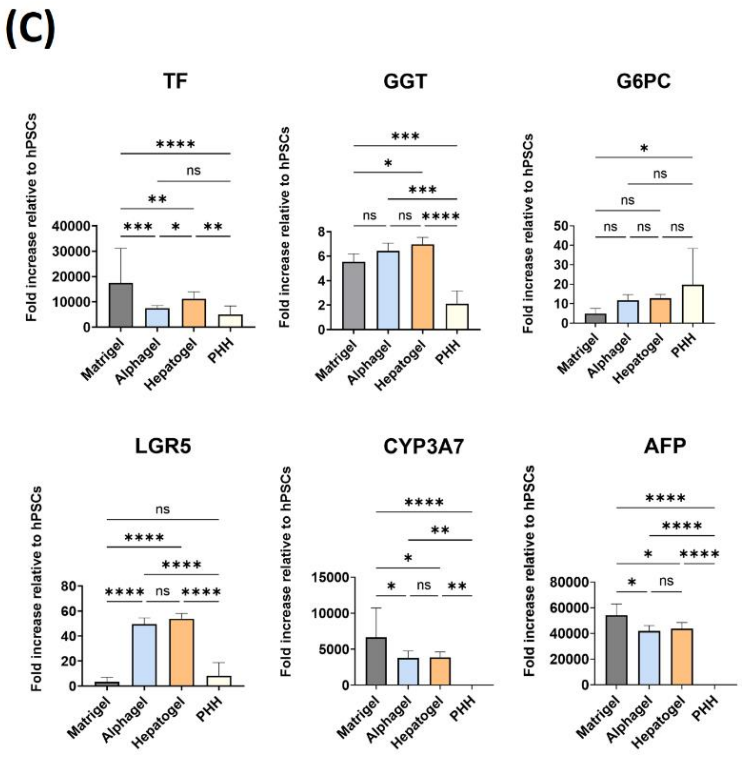

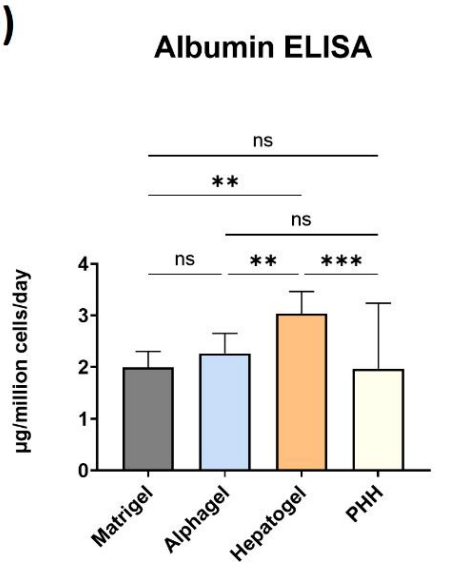

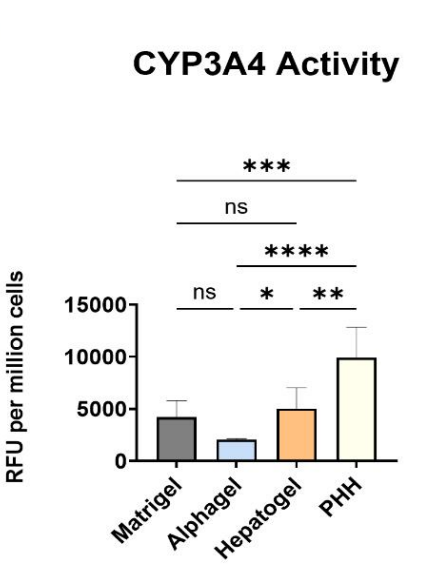

FFigure 4: (A) H&E stains of sites injected with 1% Croton Oil, Alphagel, and 0.9% Saline at 1 and 2 weeks. Black arrow denotes areas of granulation and inflammation, * denotes necrotic and degenerating muscle fibres, and # denotes supportive changes around affected muscle fibres. Scale bar = 200µm. (B) Histological grade and scores of injection sites over 6 weeks. (C) Highlighted changes in gene expression in iHeps derived with Hepatologel versus, Alphagel, Matrigel, and adult primary human hepatocytes (PHH). (D) Albumin ELISA of culture media collected from iHeps 2 days after completion of hepatic differentiation and from PHH 2 days after plating. (E) Luciferin-based measure of CYP3A4 activity in iHeps 2 days after completion of hepatic differentiation and PHH 2 days after plating. One-way ANOVA; * = $p < 0.05$, ** = $p < 0.01$, *** = $p < 0.001$, and **** = $p < 0.0001$.

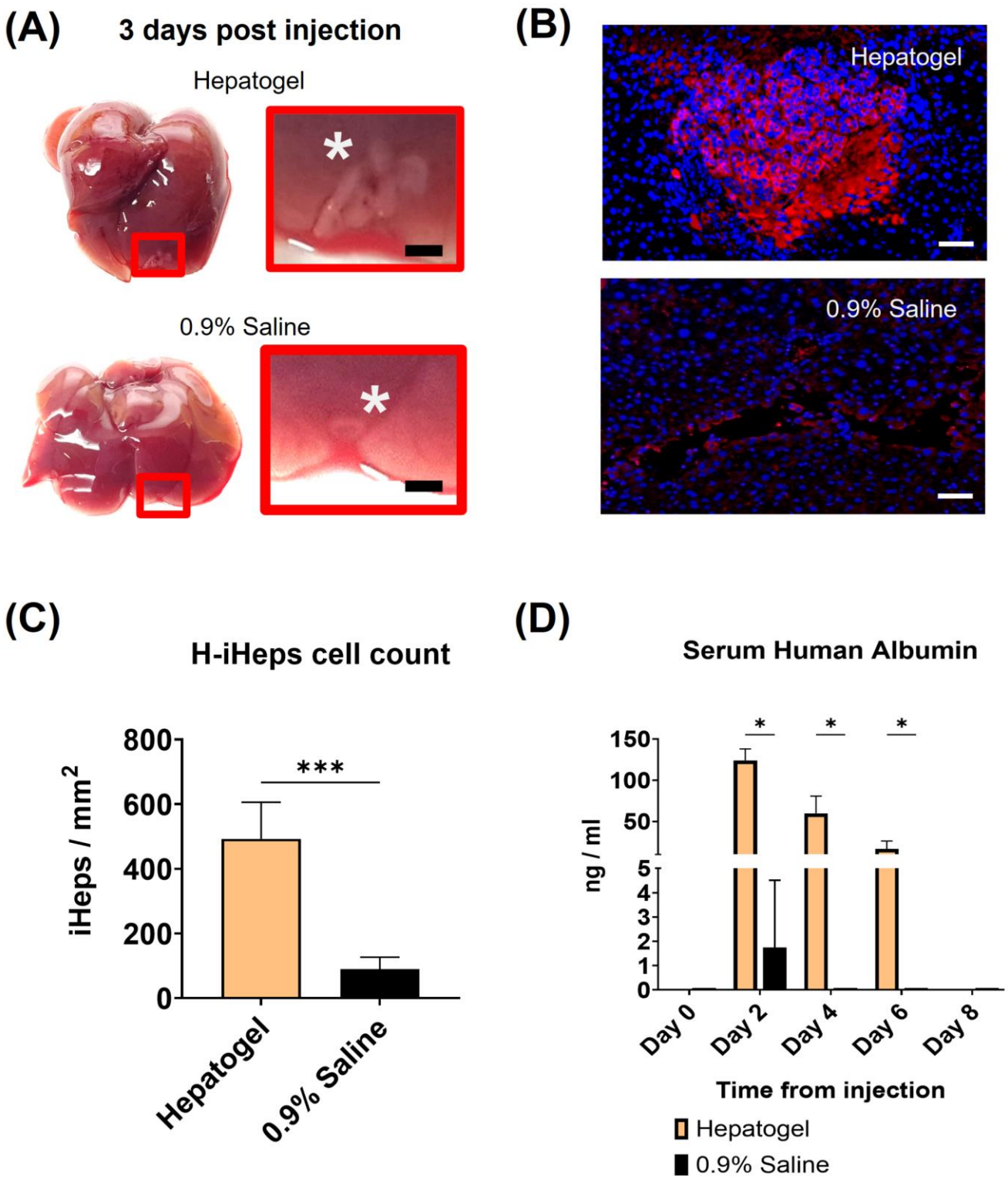

Figure 5: (A) Mouse livers excised 3 days after intra-hepatic injection with H-iHeps in Hepatogel and 0.9% saline. Red box = area magnified. * = site of injection, scale bar = 1mm. (B) Liver section and IF staining of human albumin (red) in transplanted iHeps engrafted in mouse liver 3 days after intra-hepatic injection. Scale bar = 100µm. (C) Cell counts for H-iHeps identified by albumin staining on liver histology; samples harvested 3 days after intra-hepatic injection. (D) ELISA of mouse serum for human albumin after injection with H-iHeps in Hepatogel and 0.9% saline over time. Day 0 = serum levels before injection. T-test; *** = $p < 0.001$, and **** = $p < 0.0001$

Supplementary Figure 1

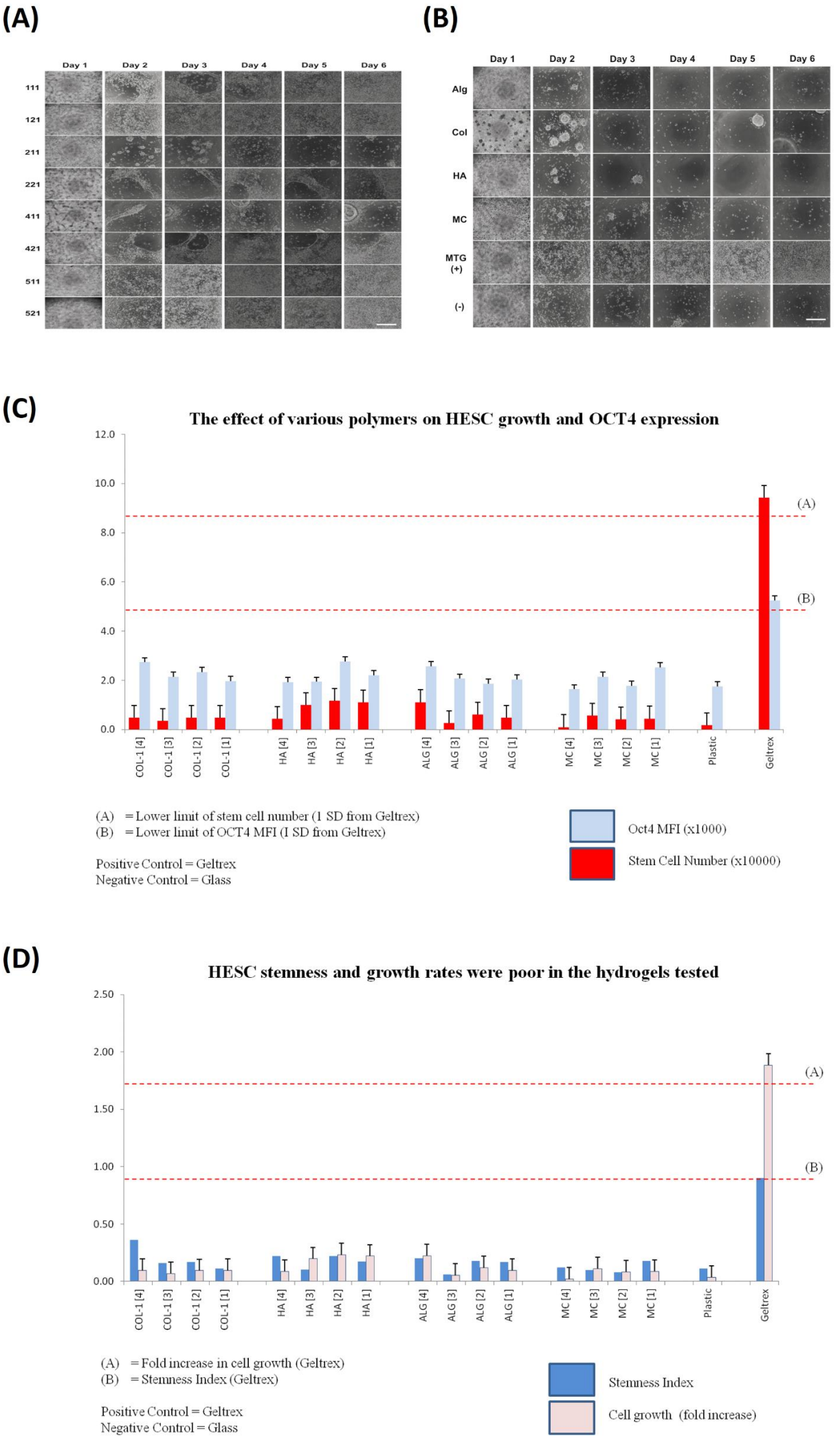

Supplementary Figure 1: Bright-field microscopy of hPSCs on (A) various laminin isoforms (y-axis) and (B) FDA-approved polymers over time (x-axis). Alg = alginate, Col = collagen-1, HA = hyaluronic acid, MC = methylcellulose, MTG (+) = Geltrex (positive control), and (-) = Tissue culture treated glass bottom plate (negative control). Scale bar = 100µm. (C) Example of OCT4 MFI with stem cell numbers, and (D) the calculated stemness index (SI) and growth rates on various hydrogel-forming FDA-approved proteins after 7 days.

Supplementary Figure 2

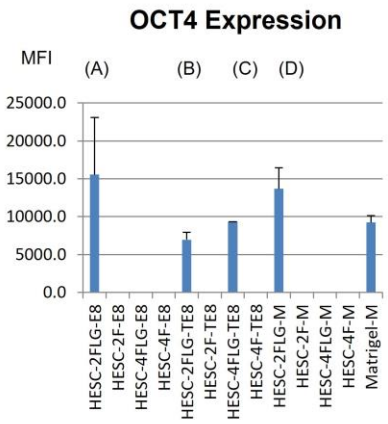

(A) vs Matrigel	p = 0.27
(B) vs Matrigel	p = 0.13
(C) vs Matrigel	Not applicable
(D) vs Matrigel	p = 0.13
Stem. Index (A)	0.62
Stem. Index (B)	0.59
Stem. Index (C)	0.87
Stem. Index (D)	1.0
Stem. Index (MTG)	0.98

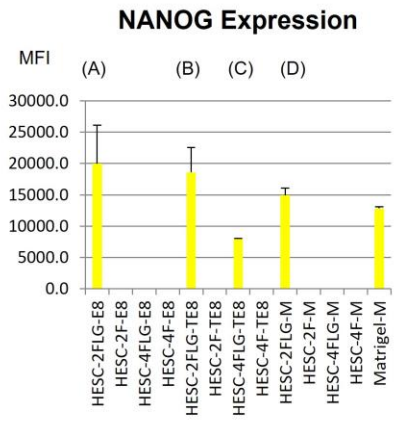

(A) vs Matrigel	p = 0.13
(B) vs Matrigel	p = 0.13
(C) vs Matrigel	Not applicable
(D) vs Matrigel	p = 0.13
Stem. Index (A)	0.98
Stem. Index (B)	1.00
Stem. Index (C)	0.54
Stem. Index (D)	1.00
Stem. Index (MTG)	1.00

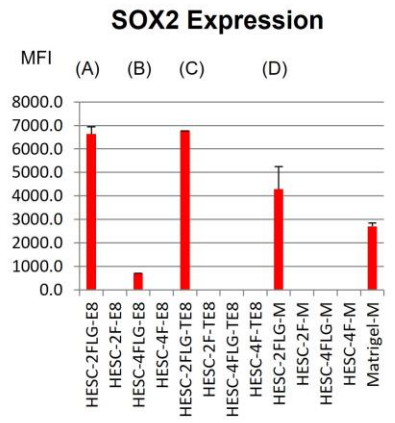

(A) vs Matrigel	p = 0.13
(B) vs Matrigel	Not applicable
(C) vs Matrigel	Not applicable
(D) vs Matrigel	p = 0.13
Stem. Index (A)	0.79
Stem. Index (B)	0.01
Stem. Index (C)	0.50
Stem. Index (D)	0.94
Stem. Index (MTG)	0.72

Supplementary Figure 2: Stem cell marker expression (MFI) presented as mean ± standard error of the mean (S.E) and stemness index (SI) in various culture conditions after 3-4 months. Bar chart x-axis label key: (i) cell type, (ii) fibrin concentration (2mg/ml or 4mg/ml), (iii) gel-type = fibrin-laminin hydrogel (FLG) or fibrin only (F), and (iv) media type = mTeSRs/TeSR2 (M), TeSR-E8 (TE8), and E8 (E8). 2FLG is representative of Alphagel. HESCs cultured in 2mg/ml fibrin gel with FLG in E8 media. The absence of bars and/or S.E. was because cells died or differentiated in other repeats and no longer expressed stem cell markers. *p* values derived using the Mann Whitney U test (MFI), Chi-square test (SI) or Fisher test (when n < 5 for any cell).

Supplementary Figure 3

(A)

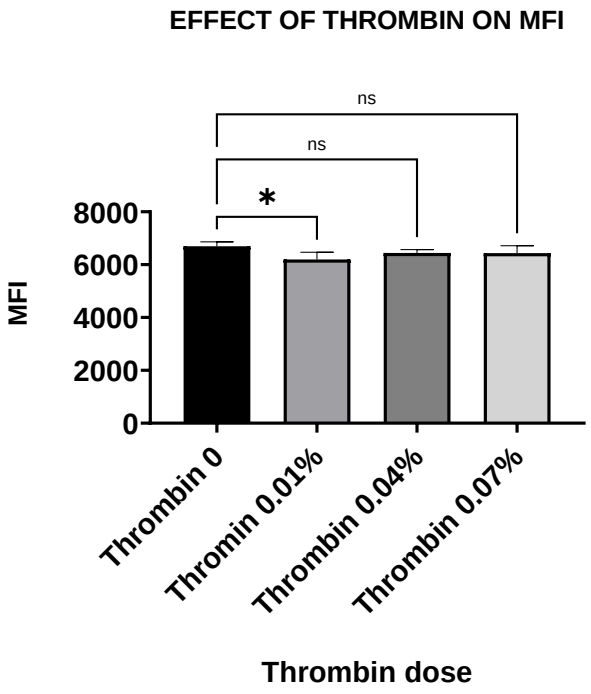

(B)

Cost analysis of Matrigel vs Alphagel in 3D cell culture

	Corning Matrigel (hESC qualified) from Fisher Scientific	Recombinant human Laminin 521 from Biolamina (**clinical grade**)	Recombinant human Laminin 521 from Biolamina (**research grade**)
Cost on Cambridge EDRS	£500.50 for 10ml (ID: 10365602)	£546.26 (ID: CT521-0501)	£364.17 (ID: LN521-05)
Unit cost (per microlitre)	5p	5.5p	3.64p
Volume used per 50ul dome	33.3ul	25ul	25ul
Cost per 50ul dome	£1.67	£1.37	£0.91
Cost of human thrombin per dome	NA	10.4p (£78.84 for 1gm)	10.4p (£78.84 for 1gm)
Cost of human fibrinogen per dome	NA	1.7p (£171.00 for 1gm)	1.7p (£171.00 for 1gm)
Total cost per dome (50ul)	£1.67	£1.49	£1.03
Cost per ml of gel	£33.40	£29.80	£20.60
Potential cost savings (vs Matrigel)	-	**10.8%**	**38.3%**

Supplementary Figure 3: (A) MFI in varying thrombin concentrations. Thrombin 0 (control) = Laminin 521 and fibrinogen without thrombin; effectively a 2D Laminin 521 coating as fibrinogen was un-crosslinked. MFI was slightly lower in 3D fibrin-laminin with 0.01% thrombin because cross-linking of fibrin with Laminin 521 was sub-optimal. Statistical comparison using One-way ANOVA, * = $p<0.05$. (B) Cost-analysis to synthesize a 50µl hydrogel dome for 3D cell culture; Alphagel vs Matrigel.

Supplementary Figure 4

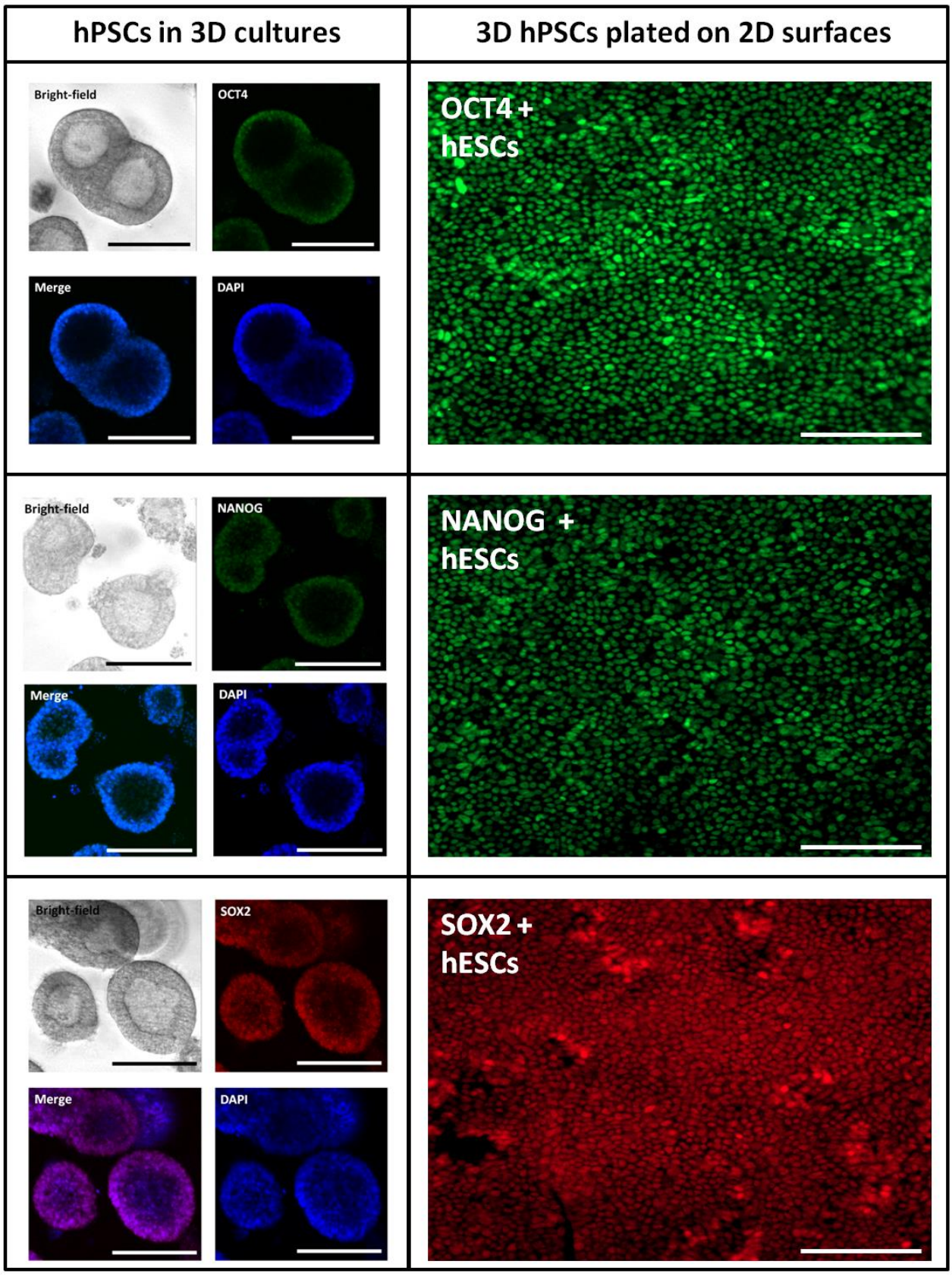

Supplementary Figure 4: Left column: Bright-field and immunofluorescent images with positive nuclear staining of hPSC in 3D. Right column: hPSCs derived from 3D cell aggregates and cultured as a 2D monolayer. Scale bar = 200μm. Cells continue to proliferate and express nuclear markers of pluripotency.

Supplementary Figure 5

(A)

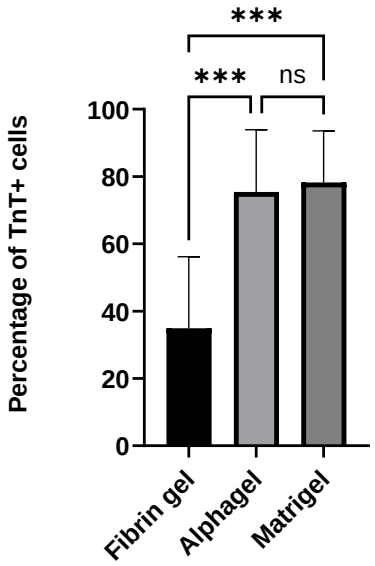

(B)

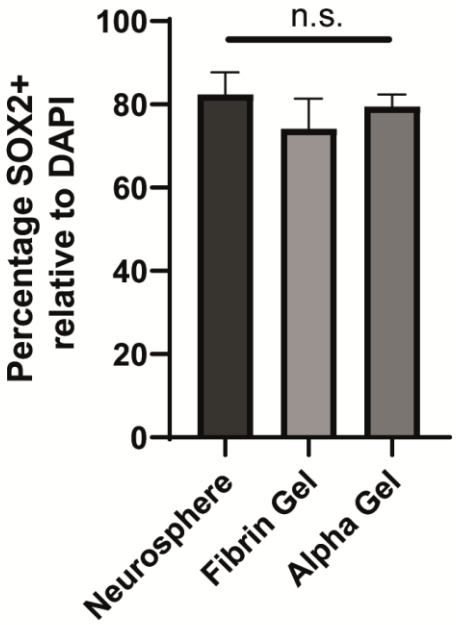

(C)

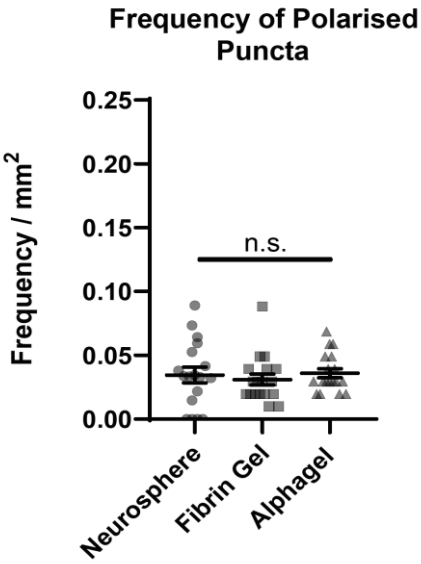

Supplementary Figure 5: (A) Percentage of Troponin T-positive cells after 14 days of cardiac differentiation. (B) Percentage of SOX2 positive neural progenitor cells and (C) the frequency of polarised neural progenitor puncta after 16 days of differentiation in neurospheres, fibrin-only hydrogel, and Alphagel. One-way ANOVA using the proportion of positive cells, *** = $p < 0.001$.

Supplementary Figure 6

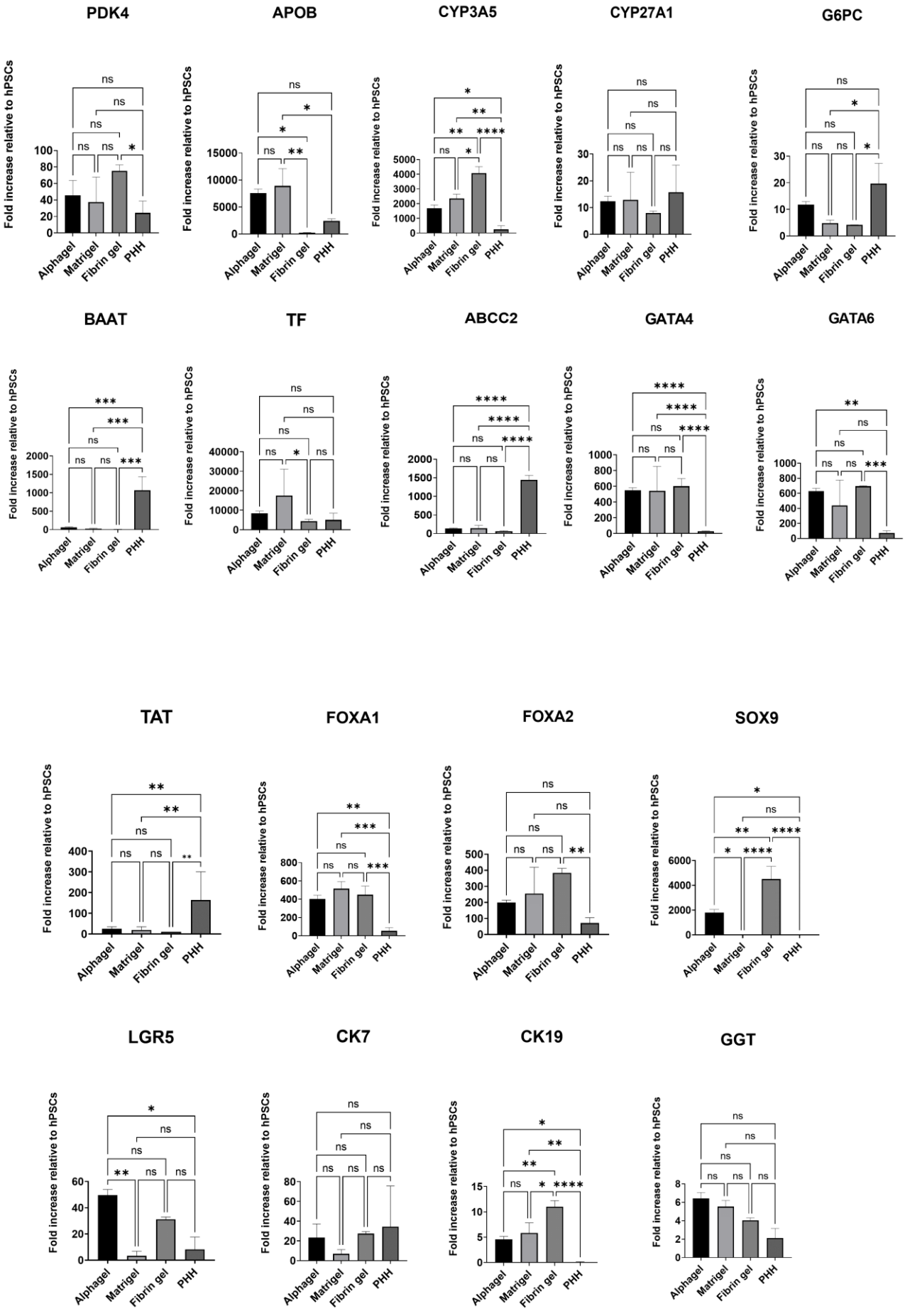

Supplementary Figure 6: Gene expression data of the remaining 18 of 24 liver-associated genes analysed.

Supplementary Figure 7

(A)

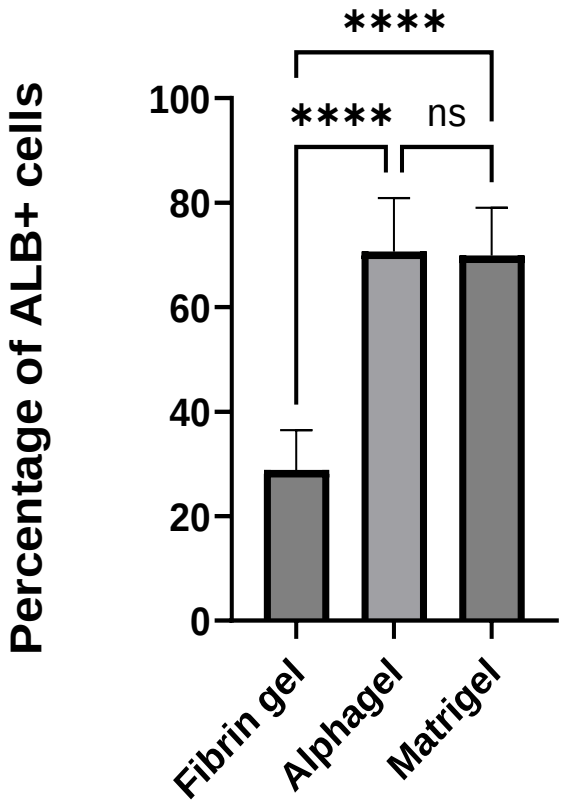

(B)

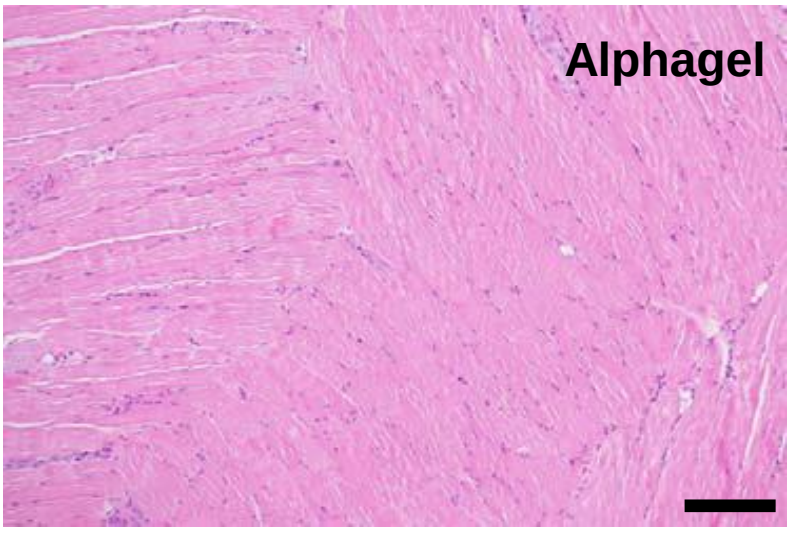

Supplementary Figure 7: (A) Percentage of Albumin-positive cells after days of hepatic differentiation. One-way ANOVA using the proportion of positive cells, **** = $p < 0.0001$. (B) Representative histology and H&E stain of Alphagel injection site after 6 weeks showing complete resolution of previously mild inflammation. Scale bar = 200µm.

Supplementary Figure 8

Microscopic lesions	Score
1. Infiltrate, inflammatory cell, Polymorphs	
2. Infiltrate, inflammatory cell, Mononuclear cells	
3. Haemorrhage	
4. Suppuration	
5. Fibrosis	
6. Myofibers degeneration/necrosis	
7. Adipose tissue necrosis	
8. Myofibers regeneration*	
9. Granulation tissue*	
Total Score	

Supplementary Figure 7: Histology scoring tool used to assess inflammation on histopathological evaluation. Each feature of inflammation is scored on an ordinal scale from 0 to 5 (0 = no abnormality, 1 = minimal abnormality, 2 = mild abnormality, 3 = moderate abnormality, 4 = severe abnormality, and 5 = marked abnormality).

Supplementary Figure 9

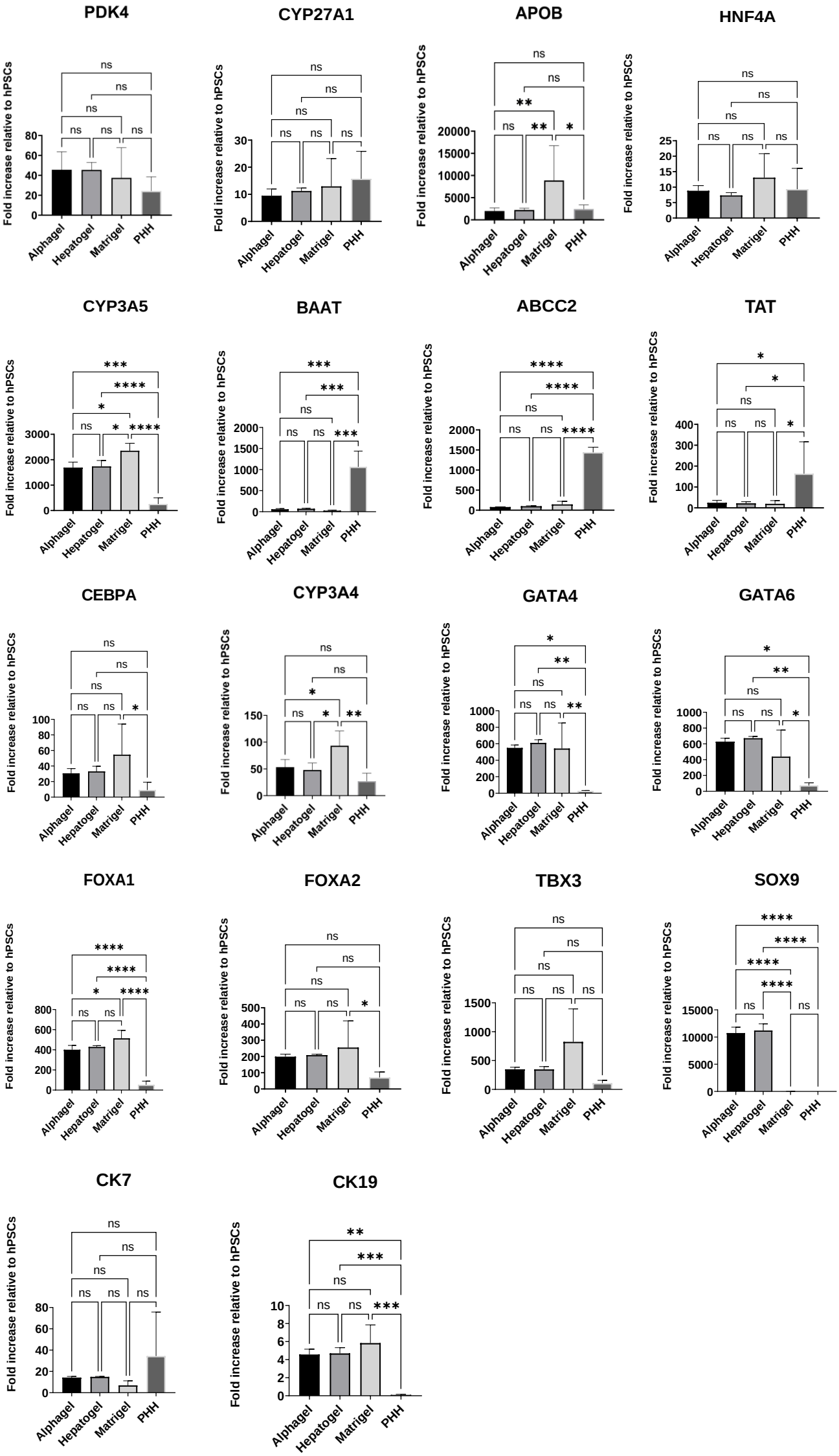

Supplementary Figure 9: Remaining gene panel of iHeps cultured in Hepatogel, Alphagel, and Matrigel vs PHH. iHeps were harvested between Day 22-24 of the hepatic differentiation process.

Supplementary Figure 10

(A)

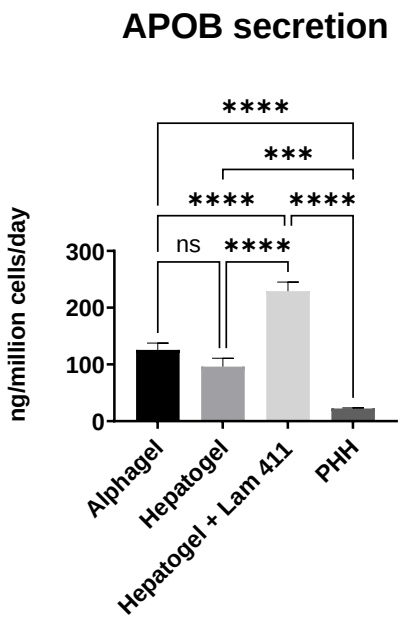

(C)

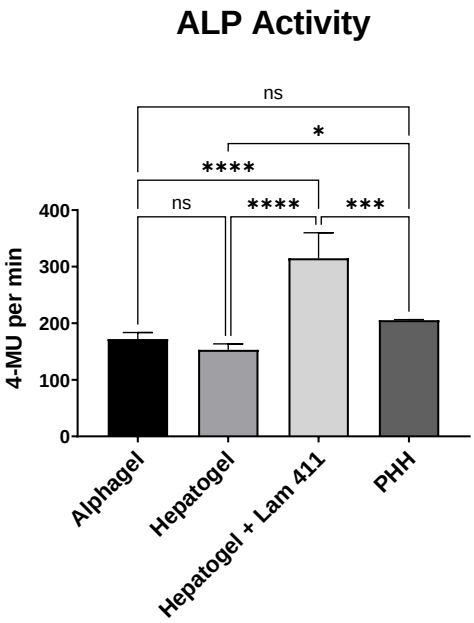

(B)

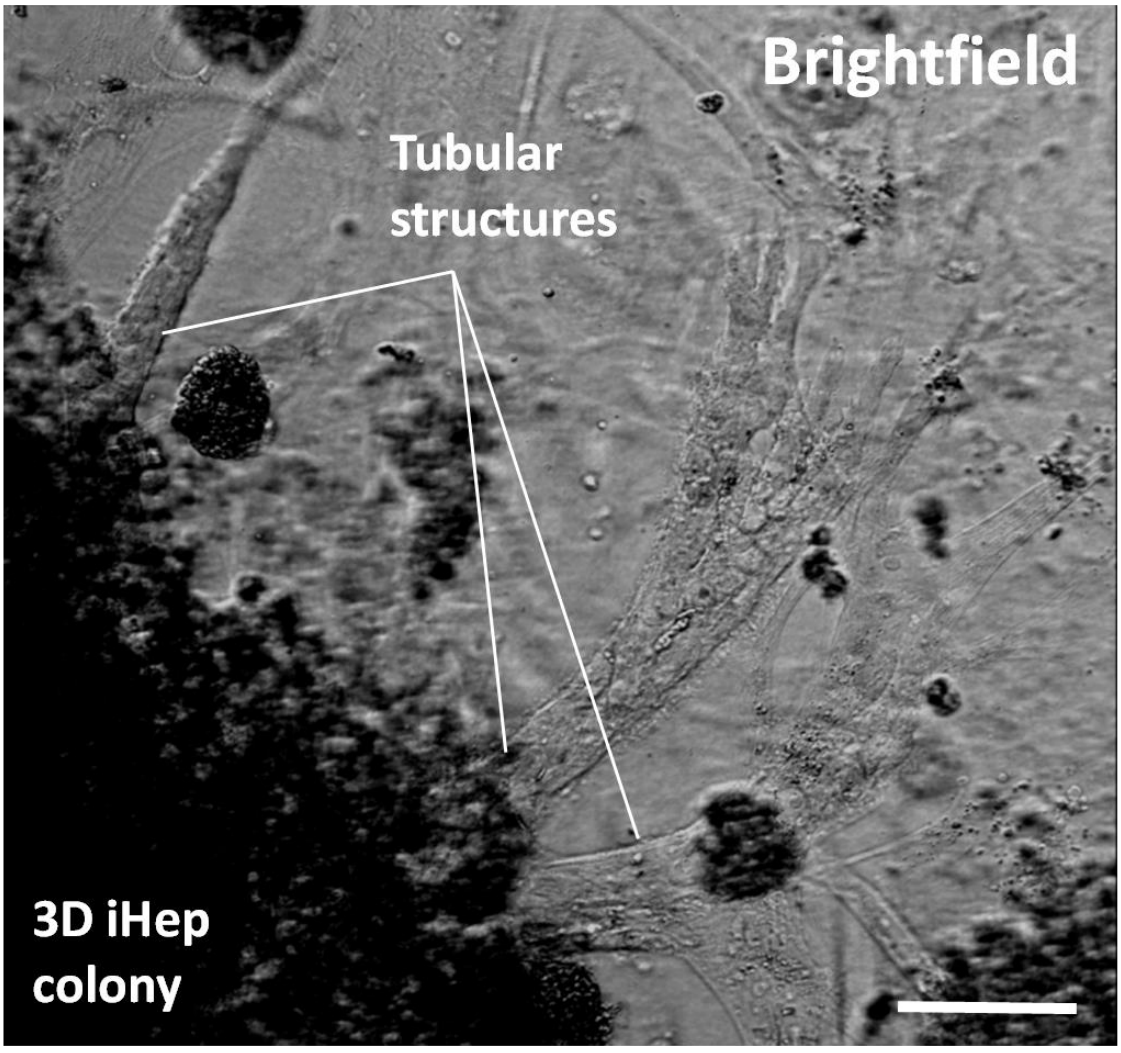

Supplementary Figure 10: (A) ELISA of culture medium for Apolipoprotein B (APOB), taken from iHeps 2 days after the end of the hepatic differentiation protocol, and from PHH culture media 2 days after plating. (B) Brightfield microscopy of 3D tubular branching strictures observed when Laminin 411 concentrations are increased. Scale bar = 100µm. (C) Alkaline Phsophatase (ALP) activity measured by colourimetric assay on culture medium taken 2 days the end of the hepatic differentiation protocol.

Supplementary Figure 11

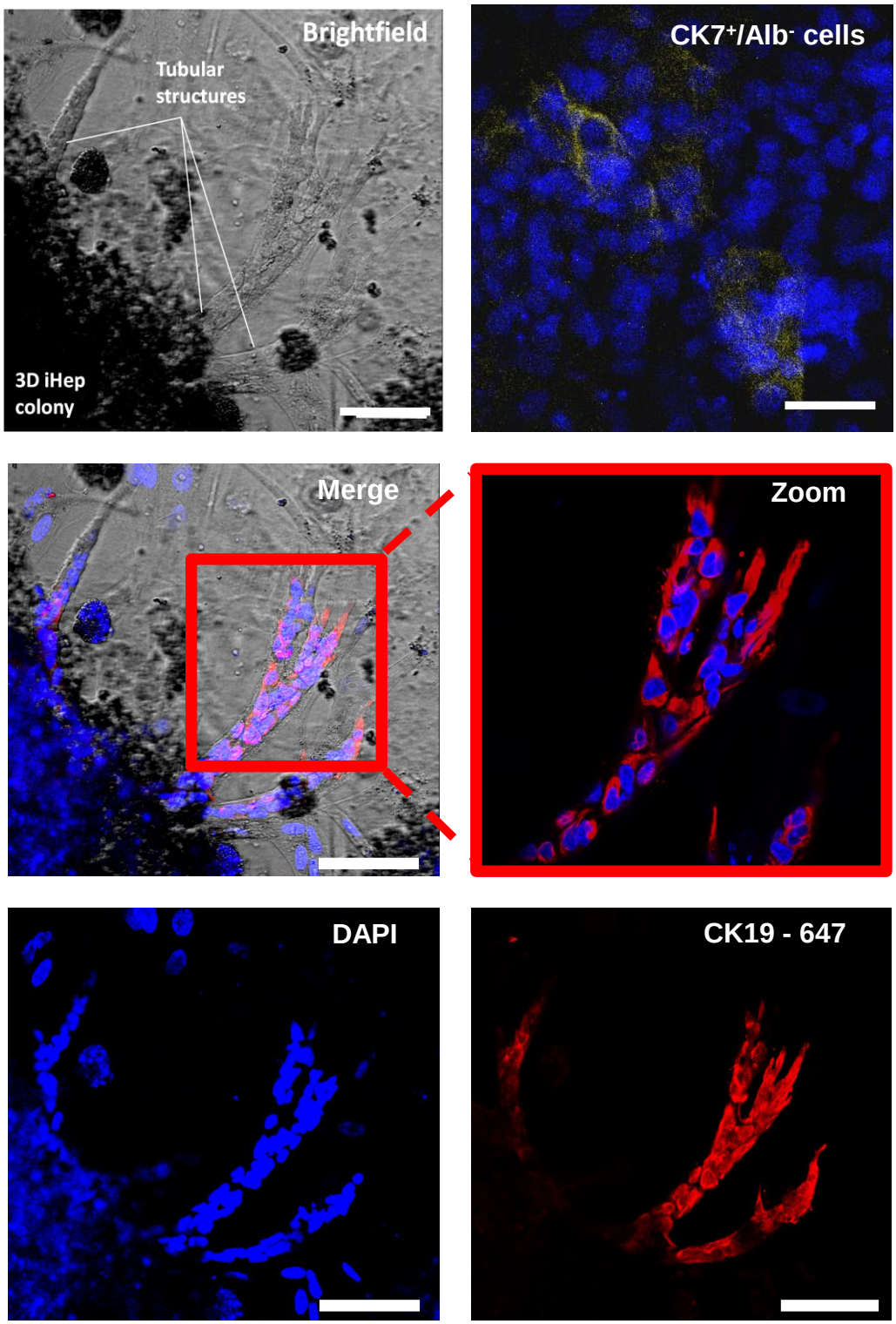

Supplementary Figure 11: Tubular structures comprising of cells that are Cytokeratin 7 (CK7) positive (yellow), Cytokeratin 19 (CK19) positive (red) and albumin negative. DAPI = blue. Scale bar = 100µm

Supplementary Figure 12

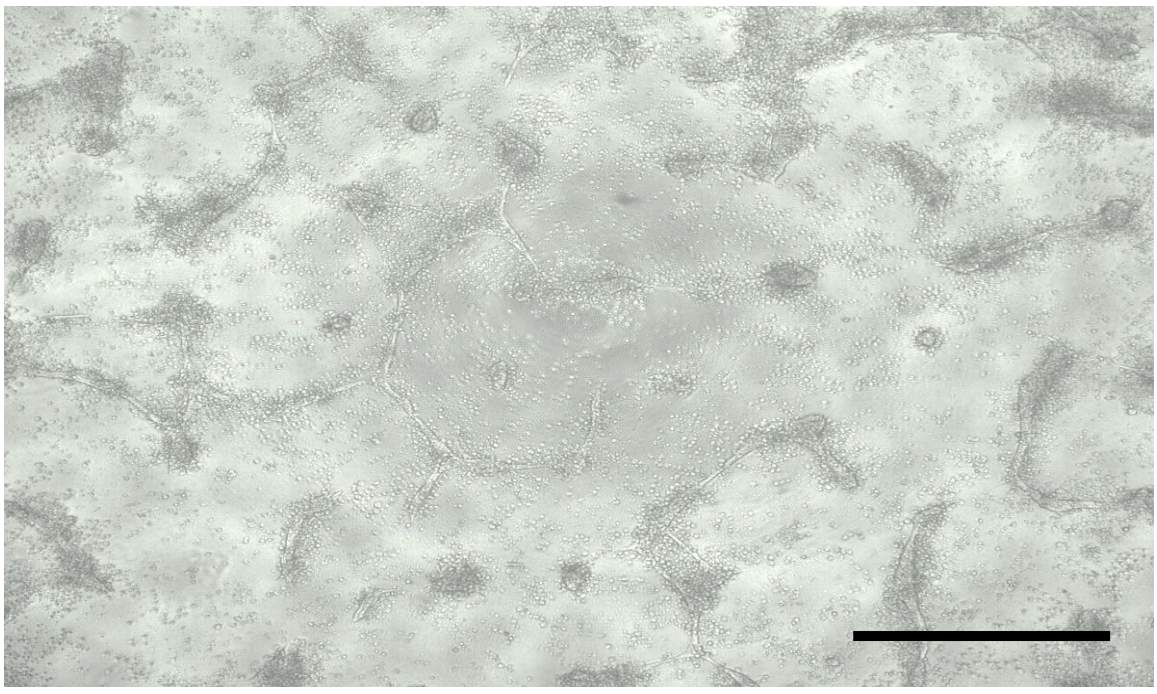

Supplementary Figure 12: Tube-like formations in hESCs on cultured on Laminin 111 with mTESR media on 2nd passage, x40 magnification. Scale bar = 250µm